# Heat and Fluid Flow Analysis in a Molten CuCl Heat Exchanger

By

Othman Jaber

A Thesis Submitted in Partial Fulfillment

of the Requirements of the Degree of

Master of Applied Science in Mechanical Engineering

Faculty of Engineering and Applied Science

University of Ontario Institute of Technology

October 2009

# Abstract

The Cu-Cl thermochemical cycle is a promising method to generate hydrogen as a clean fuel for human use in the future. The cycle can be coupled to nuclear reactors to supply its heat requirements. The cycle generates hydrogen by splitting water molecules through a series of chemical reactions. Thermal management within the cycle is crucial for improving its thermal efficiency. The cycle has an average theoretical efficiency of around 46% without any heat recovery. The efficiency may increase up to 74%, if all heat associated with the products of the cycle's steps is recycled internally. The products of the different processes that transfer heat are; oxygen, hydrogen, and molten CuCl. The heat carried by oxygen and hydrogen can be recovered by the use of conventional heat exchangers. However, recovering heat from molten CuCl is very challenging due to the phase transformations that molten CuCl undergoes, as it cools down from liquid to solid states. This thesis presents a new model that predicts the fluid flow and heat transfer in a direct contact heat exchanger, designed to recover the heat from molten CuCl, through the physical interaction between CuCl droplets and air. Numerical results for the variations of temperature, velocity, heat transfer rate, and so forth, are given for two cases of CuCl flow. The predicted dimensions of the heat exchanger were found to be a diameter of 0.13 m, and a height of 0.6 and 0.8 m for 1 and 0.5 mm droplet diameters, respectively. The results obtained provide valuable insights for the equipment design and scale-up of the Cu-Cl cycle.

Keywords: CuCl, Direct Contact Heat Exchanger, Droplet, Efficiency, Flow, Heat Recovery, Heat Transfer, Hydrogen.

# Acknowledgments

I would like to express my sincere gratitude and appreciation to my co-supervisors; Professor G.F. Naterer and Professor I. Dincer for the unique opportunity they gave me to work in this area of research, their mentorship, and guidance throughout my work.

I would also like to express my gratitude to my parents and family for their endless support and encouragement.

Financial support of this research from the Ontario Research Fund (ORF), Atomic Energy of Canada Limited (AECL), and the Natural Sciences and Engineering Research Council of Canada (NSERC) are gratefully acknowledged.

Last but not least, I would like to thank all my friends who have supported me throughout my work.

# Table of Contents

# List of Tables

# List of Figures

# Nomenclature

| | |
|---|---|
| $A_c$ | Droplet Cross-Sectional Area, $m^2$ |
| $A_d$ | Surface Area of Droplet, $m^2$ |
| $A_f$ | Cross-Sectional Area of Fluid Flow Path, $m^2$ |
| $a_d$ | Droplet Acceleration, $m/s^2$ |
| $Bi$ | Biot Number, $\frac{h\, l_c}{k_d}$ |
| $C_D$ | Drag Coefficient, $\frac{2F_D}{\rho {V_T}^2 A_c}$ |
| $C_{p\,d}$ | Droplet Specific Heat, J/kg°C |
| $C_{p\,f}$ | Specific Heat of Fluid, J/kg°C |
| $D_d$ | Droplet Diameter, m |
| $F_B$ | Buoyancy Force, N |
| $F_D$ | Drag Force, N |
| $F_R$ | Resultant Force, N |
| $F_W$ | Weight Force, N |
| $g$ | Gravitational Acceleration, 9.81 $m/s^2$ |
| $H$ | Height, m |
| $h$ | Convective Heat Transfer Coefficient, $W/m^2$°C |
| $\bar{h}$ | Average Convective Heat Transfer Coefficient, $W/m^2$°C |

| | |
|---|---|
| $k_d$ | Thermal Conductivity of Droplet, W/m°C |
| $k_f$ | Thermal Conductivity of Fluid, W/m°C |
| $l_c$ | Characteristic Length, m |
| $\dot{m}_d$ | Droplet Mass Flow Rate, kg/s |
| $m_d$ | Mass of Droplet, kg |
| $\dot{m}_f$ | Fluid Mass Flow Rate, kg/s |
| $N_d$ | Number of Droplets in Differential Element, Droplets |
| $Pr_f$ | Prandtl Number of Fluid, $\frac{\mu_f C_{pf}}{k_f}$ |
| $\dot{Q}_{convection}$ | Convection Heat Transfer Rate, W |
| $\dot{Q}_d$ | Droplet Heat Transfer Rate, W |
| $\dot{Q}_f$ | Fluid Heat Transfer Rate, W |
| $r_d$ | Droplet Radius, m |
| $Re$ | Reynolds Number, $\frac{\rho V_T D_d}{\mu_f}$ |
| $r_f$ | Radius of Fluid Flow Path, m |
| $T_d$ | Droplet Temperature, °C |
| $T_f$ | Fluid Temperature, °C |
| $v_d$ | Droplet Volume, $m^3$ |
| $V_d$ | Droplet Velocity, m/s |

| | |
|---|---|
| $V_f$ | Fluid Velocity, m/s |
| $V_{f,exp}$ | Fluid Expansion Velocity, m/s |
| $V_T$ | Total Velocity, m/s |
| $Nu$ | Nusselt Number, $\frac{hD_d}{k_f}$ |
| $\overline{Nu_d}$ | Average Nusselt Number for Droplet, $\frac{\bar{h}D_d}{k_f}$ |

# Greek Letters

| | |
|---|---|
| $\mu_f$ | Dynamic Fluid Viscosity, Pa s |
| $\pi$ | Pi Number, 3.1416 |
| $v_f$ | Fluid Specific Volume, $m^3/kg$ |
| $\rho_d$ | Droplet Density, $kg/m^3$ |
| $\rho_f$ | Fluid Density, $kg/m^3$ |

# Subscripts

| | |
|---|---|
| $e$ | Exit |
| $i$ | Inlet |
| $s$ | Surface |

# Acronyms

| | |
|---|---|
| AECL | Atomic Energy of Canada Limited |
| AHTR | Advanced High Temperature Reactor |
| CDQ | Coke Dry Quenching |
| CWQ | Coke Wet Quenching |
| HTGR | High Temperature Gas-cooled Reactor |
| HTTR | High Temperature Test Reactor |
| JAERI | Japan Atomic Energy Research Institute |
| LMTD | Log Mean Temperature Difference |
| MHR | Modular Helium Reactor |
| NSERC | Natural Sciences and Engineering Research Council of Canada |
| NTU | Number of Transfer Units |
| ORF | Ontario Research Fund |
| SCWR | Super Critical Water Reactor |
| SMR | Steam Methane Reforming |
| STAR | Secure Transportable Autonomous Reactor |
| UOIT | University of Ontario Institute of Technology |

# Chapter 1

## Introduction

### 1.1 Background

Currently 80% of the world's energy demand is supplied from fossil fuels, 14% from renewable energy resources and about 6% from nuclear energy [1,2]. These percentages will certainly change in the near future, as the world's population increases, and energy demand increases. It is expected that energy supplies from renewable and nuclear resources will grow to account for more and more of the world's energy demand, while the energy supplies from fossil fuels will decrease in the future. It is not only the increase in energy demand, which will lead to this shift in energy supply from fossil fuels to renewable and nuclear resources, but also environmental concerns and the need to take quick and sustainable action towards global warming, increases in the price of fuels derived from fossils, energy security, sustainability, and so forth. All of these reasons and many more will lead further to increasing the need for renewable and nuclear energy resources. Much effort is being devoted to utilize renewable energy around the world. This can be seen by the increased research and funding for such programs. Another growing effort is to develop nuclear power plants around the world, which can be seen by the increasing number of countries that are adopting nuclear energy programs. But in the future, all energy producing systems will be hybrid systems, a mixture of different energy resources and energy conversion methods to exist as one system. This will maximize

the process or cycle efficiency, make the process or cycle environmentally friendly and therefore reduce the impact on the environment to a minimum. It will have less environmental impact, and make energy systems sustainable. One key link between renewable and nuclear energy resources utilized in hybrid systems, when considering a sustainable and environmentally friendly fuel for the future, is hydrogen.

Hydrogen itself is not an energy resource, but instead an energy carrier [2,3]. Hydrogen can be viewed as a link between the different energy resources and society, in an energy chain connecting the energy resources to the final use or service. This link will provide society with the various services it will need; such as heating, transportation, manufacturing, etc. In the end, it is this energy carrier that will matter for societies, not the energy source that is used to produce it. Hydrogen is independent of the source used to produce it. It can be produced from a wide variety of sources. Hydrogen is environmentally friendly; no greenhouse gas emissions are produced upon burning it [3]. It also exists in large quantities in the world; in water for example, where water makes up about two thirds of the earth. So it is readily available, and it can be used as a fuel in already existing technologies, such as transportation, where only slight modifications have to be made to the already existing engines to operate on hydrogen. This will make the transition from fossil fuel technologies to the new renewable and nuclear technologies easier. Finally, hydrogen can be used relatively safely in society, and it is easy to handle and use by people with no great risk relative to other fuels in sectors like transportation applications. For all of these reasons, hydrogen is considered the best alternative to fossil fuels as an energy carrier for future energy supply and environmentally friendly technologies.

Many methods and technologies currently exist for producing hydrogen. However, most of them are based on reforming fossil fuels and thus emit carbon

dioxide to the atmosphere [2,4,5]. Reforming of fossil fuels to produce hydrogen accounts for more than 78% of the world's total hydrogen production, with natural gas and petroleum products accounting for 48% and 30%, respectively, of the total production [2,5]. Water electrolysis is also currently used to produce hydrogen. It accounts for about 4% of the world's total hydrogen production. It is considered an environmentally friendly method. However, it is a very energy intensive method and has low efficiencies, especially when the efficiency of the generated electricity is taken into account. Thermochemical water splitting cycles are a clean, more efficient and thus promising alternative to produce hydrogen, as they can be coupled to all types of energy sources (e.g., solar, geothermal and conventional fossil fuels). They can also be coupled with nuclear power plants to utilize their waste heat [6,7]. Currently, most of the research being conducted on the use of Cu-Cl and S-I cycles with nuclear power plants require heat at a maximum temperature of 530°C, for the Cu-Cl cycle, and 900°C, for the S-I cycle.

The Canadian hydrogen demand in 2004 was 2.88 million tons. Most of it was used by petrochemical industries, either internally in oil refineries, or to upgrade heavy oil fuels. Canadian hydrogen demand is expected to grow to 6 million tons per year by 2023, where about 50% of it is expected to be used to upgrade heavy oils [8].

Steam methane reforming (SMR) has been studied extensively, since it is the main method of hydrogen production. Detailed thermodynamic analysis, energy and exergy, for SMR can be found in many references [4,6,7,9]. Thermochemical hydrogen production methods are still in the development stage. They can be coupled to all types of energy sources. They offer great flexibility and can be sustainable. The Cu-Cl cycle is one of great importance in Canada, as it is the selected cycle for nuclear based hydrogen production by Atomic Energy of Canada Limited (AECL).

The goal of this cycle is to couple it to the next generation of CANDU nuclear reactors to produce hydrogen. The S-I thermochemical cycle is being developed by the USA, Japan, and others. It would be linked with high temperature nuclear reactors, with temperatures up to 900°C.

## 1.2 Motivation and Objectives of Thesis

Currently, a research team led by Dr. G.F. Naterer at the University of Ontario Institute of Technology (UOIT) is developing a lab-scale demonstration of the Cu-Cl cycle. The research is in collaboration with Atomic Energy of Canada Limited (AECL), Argonne National Laboratory in the U.S. and other partners. The aim of the collaboration is to demonstrate and show that hydrogen can be produced efficiently without any greenhouse gas emissions using the Cu-Cl cycle.

One of the main challenges for this cycle to be industrially adopted and used for mass hydrogen production is to convince the public and decision makers that it is a better alternative to current well established hydrogen production methods, not only from an environmental point of view, but also from an economic perspective. The Cu-Cl cycle can outperform current hydrogen production methods, such as steam methane reforming and coal gasification, environmentally, when it is coupled to clean energy resources, such as renewables and nuclear. This will lead to a zero emission method of efficient hydrogen production. The Cu-Cl cycle also has major advantages over its competitor, the thermochemical S-I cycle, when coupled to renewable or even nuclear resources, as it requires a maximum temperature of 530°C compared to 900°C. This gives it the advantage of requiring less complex and expensive systems to be coupled with renewable resources, and also the ability to be coupled with existing nuclear reactors of all types that can produce heat at the maximum required

temperature. In contrast, the S-I cycle is designed to be coupled to the next generation of high temperature gas cooled reactors that produce heat at temperatures over 900°C. This gives the Cu-Cl cycle much better flexibility than the S-I cycle.

In order for the Cu-Cl cycle to outperform current hydrogen production methods economically, then it has to be coupled to cheaper sources of energy and make the maximum use of the supplied heat. The latter point is of great importance for success of the Cu-Cl cycle. Energy analysis and studies of the Cu-Cl cycle have shown that it has an efficiency of 46% [10], without considering any heat recovery within the cycle. This efficiency is lower than other hydrogen production technologies; for example, steam methane reforming plants have an efficiency of around 66% [9]. So for the Cu-Cl cycle to out-perform other hydrogen production cycles in terms of efficiency, the recovery of heat within the cycle has to be optimized. Naterer et al. [10] have shown that the cycle efficiency can be raised significantly if all heat is recovered within the cycle.

The objective of this thesis is to show how the heat from molten CuCl, which is a direct product from the oxygen and hydrogen production steps, can be recovered and recycled within the Cu-Cl cycle, by a direct contact heat exchanger, to increase its efficiency. The specific objectives can be summarized as follows:

- To design a direct contact heat exchanger to recover heat from molten CuCl, produced by a CuCl pilot plant operating with a capacity of 3 kg of hydrogen per day.
- To study the fluid and droplet flows and heat transfer phenomenon within the heat exchanger.
- To study the effect of the droplet size on the heat exchanger's dimensions.

- To find the flow configurations that satisfy the model's assumptions for each droplet size examined.

The molten CuCl from the oxygen and hydrogen production steps has temperatures of around 530°C and 450°C, respectively. When recovered, it is enough to supply about 30% of the total heat requirements of the cycle. Total heat recovery from all steps is enough to supply about 42% of the total heat requirements of the cycle, including the low grade heat for preliminary heating and drying purposes. Recovering heat from the products of all steps, except from the molten CuCl, is easier, because it involves the use of conventional heat exchangers, since the products are in the gas phase. However, recovering heat from the molten CuCl is much more difficult, because the process involves phase change, from liquid to solid. In this thesis, a direct contact heat exchanger is designed and the heat transfer phenomenon is analyzed. The heat exchanger design is relatively simple, as it is basically a tube where air is blown in from the bottom, and the molten CuCl is sprayed at the top to fine droplets. The droplets fall under gravity and interact with the upcoming air that recovers heat from them. A mathematical model, which describes the heat transfer, fluid and droplet flow processes, will be developed and then solved numerically, using MATLAB. The results show how the different parameters vary throughout the heat exchanger, and the effects of various parameters on the overall heat exchanger performance and design.

# Chapter 2

## Literature Review

### 2.1 Hydrogen

Hydrogen is a promising clean fuel for future transportation and industrial use. It has a high energy content per unit mass of 140.4 MJ/kg, the highest of all known fuels. Hydrogen is considered a clean energy resource, as it does not emit any greenhouse gases upon combustion, and therefore it is widely believed that it will eventually replace fossil fuels as a source of energy for society and industry. The key criteria for an ideal fuel are inexhaustibility, cleanliness, convenience, and independence from foreign control [5]. Hydrogen potentially has all of these properties, as mentioned earlier, since it does not produce any greenhouse gases upon combustion. It can be readily available, as hydrogen can be found in many materials on earth, especially water. It can be produced almost anywhere, which means that no long transportation lines or routes are needed, and therefore the time and energy to transport regular fuels derived from fossils are saved. Finally, since the main source of hydrogen is water, any country that has access to water (e.g., rivers, lakes and seas) can have access to hydrogen without concern of foreign interference.

Hydrogen exists as $H_2$ molecules. The molecule size is smaller than any other known molecule, because the hydrogen atom has the smallest size of all known atoms. Hydrogen is colorless, odorless and tasteless. It diffuses faster than any other gas, which makes hydrogen use in transportation safe. It would diffuse into the

atmosphere before it can catch fire in case of an accident. At standard ambient conditions, hydrogen exists in the gaseous phase. It condenses to liquid at -253°C and to solid at -259°C [5].

Hydrogen has other unique properties that make it favorable when used as a fuel for current engine technologies. The flammability range for hydrogen is wide, much wider than that of gasoline, which means that it can be used as a fuel in internal combustion engines and stay stable even at the most dilute conditions possible. Hydrogen has a very high flame speed. At the stoichiometric ratio, it has a flame speed of 3.46 m/s, which is almost ten times higher than the flame speed of gasoline. This means that an engine running on hydrogen will approach the ideal Otto thermodynamic cycle [5].

## 2.2 Hydrogen Production

Hydrogen can be produced from a wide range of processes, i.e. reforming of fossil fuels, electrolysis, thermochemical water splitting and biological hydrogen production methods. Also, hydrogen can be produced from a wide range of energy sources, fossil fuels, renewables and nuclear. Currently, SMR is the most widely used process to produce hydrogen, followed by other reforming methods. These hydrogen production methods produce large amounts of carbon dioxide, which is harmful to the environment. This explains why much work has been devoted to finding new environmentally friendly methods. Among the best alternatives are the thermochemical cycles, particularly the Cu-Cl and S-I cycles.

Figure 2.1 shows the different methods used to produce hydrogen, along with the energy resources that are suitable for each method. Not all of the methods exist at an industrial size, as most of them are limited to lab scale demonstration plants. The

following is a brief review of the main hydrogen production methods, along with new more promising methods.

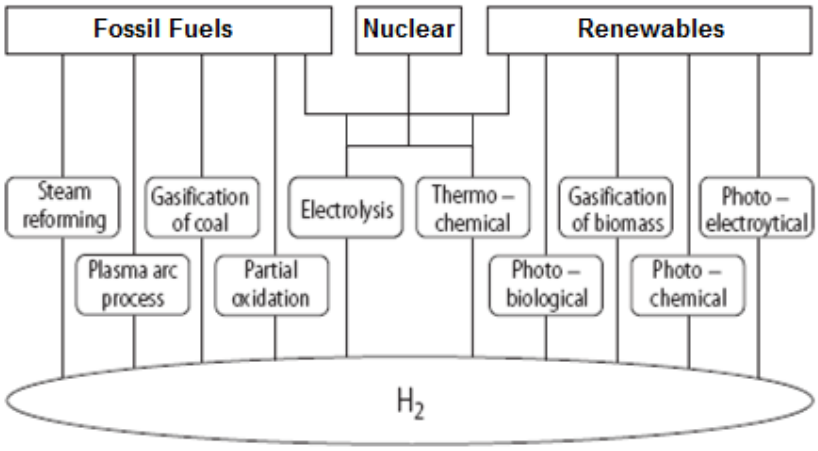


Figure 2.1 Hydrogen production methods (modified from [11]).

### 2.2.1 Steam Methane Reforming (SMR)

Worldwide production of hydrogen was about 50 million tons per year in 2003 [2]. About 48% was produced by SMR [5]. The input fuel to the process is natural gas, or simply methane, as it makes up approximately 90% of natural gas. The input fuel reacts with steam in a series of steps to produce hydrogen and carbon dioxide as products. A SMR process is made up of four basic steps; desulfurization, catalytic reforming, CO conversion, and gas separation or purification. In the desulfurization unit, the incoming natural gas is scrubbed on a ZnO bed to remove the sulfur from it, as shown by the following chemical reaction. This is done due to the high sensitivity of the reforming catalysts to sulfur.

$$H_2S + ZnO \rightarrow ZnS + H_2O \qquad (2.1)$$

After the desulfurization unit, natural gas enters the reforming reactor where it reacts with steam to produce synthesis gas at a temperature of around 850-900°C, at a pressure above 2.6 MPa, to increase the hydrogen yield. This reaction is an endothermic reaction. It requires a heat input of 206 kJ/mole of natural gas. The reaction proceeds according to the following equation.

$$CH_4 + H_2O \rightarrow 3H_2 + CO \quad (2.2)$$

The products of the reforming step along with steam enter the CO conversion unit, which is made up of two steps; low temperature water gas shift reaction step, and high temperature water gas shift reaction step. In the CO conversion unit, the produced CO reacts with steam to produce more hydrogen according to the following reaction.

$$CO + H_2O \rightarrow H_2 + CO_2 \quad (2.3)$$

The CO conversion reaction is carried out in two steps to ensure that all incoming CO is converted to carbon dioxide. The CO conversion reaction is an exothermic reaction that produces heat at a rate of 41.2 kJ/mole of CO. Finally, the gas mixture of $H_2$ and $CO_2$ enters the gas separator, where both gases are separated from each other by using solvents to absorb the carbon dioxide [5].

SMR has been studied extensively by many authors, since it is the most widely used method to produce hydrogen. Rosen [4] analyzed steam methane reforming thermodynamically. The analysis determined the energy and exergy efficiencies of steam methane reforming. The performance of the plant was investigated by examining the flows of energy and exergy through the various steps of the process. A

process description was presented, along with the different operating conditions. Then the energy and exergy efficiencies were found for each step in the process. The study concluded with an energy efficiency of the process of 86% and an exergy efficiency of 79%. The analysis indicated that the main exergy losses occurred in the reformer, due to the irreversibilities associated with combustion and heat transfer across large temperature differences. The losses associated with cooling water and stack gas emissions, although significant on an energy basis, are relatively insignificant on an exergy basis.

Simpson et al. [9] also studied the performance of hydrogen production via steam methane reforming. The performance was evaluated using exergy analysis, with emphasis on exergy flows, destruction, waste, and efficiencies. A model for the steam methane reformer was developed using a chemical equilibrium model with detailed heat integration. The operating parameters of the reformer were varied to illustrate their influence on the system's overall performance. The study found that the energy and exergy efficiencies of the plant were 67% and 63%, respectively, for a base case. The majority of the exergy destruction occurred in the reformer, which was due to the high irreversibility of combustion and heat transfer, and the water to steam heat exchanger. The study concluded that there is a significant amount of unused exergy within the system, up to 37% of the total input exergy, 81% of which is destroyed within the system and 19% leaving with the exhaust stream. The study also concluded that the optimal efficiency of the system is achieved when the reformer is operating at a temperature of 674°C.

Jong et al. [12] modeled the natural gas conversion process within the reformer by both chemical reaction and heat transfer models. The models gave data of the temperature, heat transfer and concentrations of hydrogen, carbon monoxide and

natural gas, along the reformer reactor. The simulated temperatures were validated with measured data from a prototype reformer. Then the model was used to evaluate the performance of six different reactor design modifications, in order to optimize the reactor. The study concluded that the hydrogen yield can be increased by 10%, by increasing the air fraction in the burner fuel by 50%. The study also found that increasing the insulation by 50% of the reformer will result in an increase of hydrogen yield of 11%. This will lead to a better temperature distribution within the reformer.

### 2.2.2 Coal Gasification

Coal is the most abundant fossil fuel on earth, and it is expected to continue to be an important source of energy for the future. Currently 23% of the world's total energy comes from coal [5]. The primary method for producing hydrogen from coal is to gasify coal in a process called coal gasification. It is a well established technology, however it is not widely used because it is not yet economically competitive to steam methane reforming. In coal gasification, coal enters a gasifier and reacts with air and steam at temperatures in the range of 1300-1500°C. In the gasifier, the following chemical reactions take place.

$$C + O_2 \rightarrow 2CO \quad (2.4)$$

$$C + H_2O \rightarrow H_2 + CO \quad (2.5)$$

The first reaction is the coal combustion reaction. However, not enough air is supplied to the coal to complete the reaction and produce $CO_2$. The products react with steam in the same manner as the CO conversion unit of a steam methane reformer to produce hydrogen. The second reaction is called the steam gasification reaction, were

steam reacts with coal at high temperatures to produce hydrogen and carbon monoxide, which will react with steam to produce further hydrogen. In practice, a coal gasification plant is very complex, involving many more components than a steam methane reforming plant.

Watanabe et al. [13] modeled the entrained flow coal gasifier. The purpose of the model was to predict the coal gasification of an entrained flow coal gasifier, and develop a technique for the design and performance optimization of coal gasifiers. The model is composed of a pyrolysis model, char gasification model, and a gas phase reaction model. A simulation of a 2 ton/day coal gasifier was preformed. The gasifier performance and the influence of different parameters on the gasifier operation were found for seven different cases. Finally, the results of the simulations were compared to experimental results to validate the model. It was found that the simulation results coincide well with the experimental data, which validated the gasifier model. The efficiency of the cold gasifier was found to be around 50-60% for the seven cases. The model also provided the temperature distribution along the height of the gasifier, which is usually hard to measure experimentally.

Yang et al. [14] performed field tests for several underground coal gasification sites in China. The purpose of their tests was to investigate the reliability of using underground coal gasification to generate hydrogen and develop methods to improve their operation. The main parameters that were measured on site are the temperature distribution throughout the gasifier, and its variation with time, hydrogen concentration along the gasifier, and the average cycle time ratios when switching from forward to backward gasification. After analyzing the experimental data, it was found that the daily water gas production is about 16,000 $m^3$, with a maximum output of 32,000 $m^3$, hydrogen content in the range of 40-70%, and a carbon monoxide and

methane content of around 6%. The results showed that two-stage underground gasification with multi-point air feed improves the average temperature distribution throughout the gasifier, and reduces the cyclical time, which increases the gasifier output. The results also showed that backward gasification forms temperature distributions in the gasifier that increase the gasification efficiency. It was shown that underground coal gasification is a feasible method to generate hydrogen.

### 2.2.3 Water Electrolysis

Water electrolysis has been known for over 200 years. It is one of the main methods of producing hydrogen by splitting water. Electrolysis is achieved by passing an electric current through water. This will dissociate the water molecules into positive hydrogen ions and negative oxygen ions. The positively charged hydrogen ions move towards the negatively charged cathode, where a reduction reaction takes place and hydrogen gas is produced. The negatively charged oxygen ions move towards the positively charged anode, where an oxidation reaction takes place and oxygen gas is produced. The overall reaction in the electrolytic cell is shown as follows.

$$2H_2O + \text{Electricity} \rightarrow 2H_2 + O_2 \qquad (2.6)$$

Water electrolysis is mainly used on a lab scale to generate hydrogen with high purity. Electrolytic cells can have very high efficiencies, up to 100% in the case of high temperature electrolysis [15]. However, when considering the electric power generation efficiency to find the overall efficiency of the process, the efficiency of

electrolyzing water is low. Also, electrolytic cells use precious catalysts, therefore their cost is usually high.

Brisse et al. [16] have investigated the performance of a solid oxide fuel cell operating in electrolysis mode at high temperatures over an operation period of 160 hours. The operating performance of the cell was found as a function of different operating parameters; temperature, humidity and current density. Measurements of the current and voltage of the cell were used to identify the different loss terms in the cell, from the electrolyte resistance and the electrode processes. The operating electrical to hydrogen efficiency was found to be 100%, when the gas outlet temperature was equal to the steam inlet temperature to the cell, when operating at cell voltages of 1.0 and 1.25 V at a current density of 1 $A/cm^2$, and a temperature of 900 and 800°C. Also, no aging of the cell was detectable as a result of the mode of operation, and changes in temperature, current density and humidity.

Shimizu et al. [17] proposed a novel method of hydrogen production by water electrolysis using an ultra-short-pulse power supply technique. The method of supplying a short pulse of power can be achieved by the use of a static induction thyristor, and a specific circuit that is called the inductive energy storage circuit. The ultra-short-pulse hydrogen generation technique is different from conventional direct current electrolysis, which relies on the diffusion limiting mechanism to generate hydrogen. The main finding of the experimental results was to show that ultra-short-pulse power can be used to electrolyze water and generate hydrogen when passing an electrical pulse through the cell for about 300 ns. This means that hydrogen generation can be achieved by the electron transfer limiting mechanism too.

Stojic et al. [18] used ionic activators in alkaline aqueous electrolytes to reduce the energy consumption of the electrolytic cell. Two types of activators have

been examined; both are ethylenediamine complexes of cobalt. A set of experiments was carried out to determine the effect of using the activators on the energy requirements of the cell, at different current densities and temperatures. The results were compared to the operating characteristics of the cell when using a standard electrolyte. It was found that the use of the activators reduces the energy input to the cell by about 10% per unit mass of electrolytically evolved hydrogen.

### 2.2.4 Sulfur-Iodine Cycle

The sulfur-iodine thermochemical cycle is one of over 250 proposed cycles. In these thermochemical cycles, water is thermally decomposed in a series of chemical reactions that lead to the production of hydrogen and oxygen, with the remaining chemicals and products being recycled internally within the cycle. Thermochemical cycles can operate with any known energy source, however, they have been primarily developed and designed to be coupled to nuclear reactors to utilize the generated heat from the reactor. Most of the thermochemical cycles have not been demonstrated to have economic viability [19]. Only a few have been shown to be very promising, such as the S-I and Cu-Cl cycles.

The sulfur-iodine cycle was developed by General Atomics Corporation in the mid 1970s [20]. The Japanese Atomic Energy Research Institute (JAERI) has also been active in developing their own version of the cycle [21]. The basic cycle involves three reaction steps as shown below.

$$H_2SO_4 \rightarrow SO_2 + H_2O + 1/2O_2 \quad (2.7)$$

$$I_2 + SO_2 + 2H_2O \rightarrow 2HI + H_2SO_4 \quad (2.8)$$

$$2HI \rightarrow I_2 + H_2 \quad (2.9)$$

The three reactions are carried out in three different compartments. The first reaction is a sulfuric acid decomposition reaction that occurs at temperatures around 900°C, which is an endothermic reaction. The second reaction is called the Bunsen reaction. It is an exothermic reaction that occurs at temperatures over 100°C. Iodine and sulfur dioxide react in an aqueous solution to produce sulfuric and hydriodic acids, which are required by the first and last reactions in the cycle. Finally, the third reaction is the hydriodic acid decomposition reaction to produce iodine and hydrogen. This is an endothermic reaction that occurs at temperatures of around 450°C. The net reaction from the S-I cycle is the splitting of water to hydrogen and oxygen [22].

The S-I cycle has many challenges to overcome, including a very high operating temperature and the corrosive acids within the cycle. These increase the cycle capital cost and maintenance costs throughout the cycle life. This cycle is being developed to be coupled to high temperature nuclear reactors, such as gas cooled nuclear reactors. Other nuclear reactor technologies exist that can be used to produce hydrogen at high temperatures. The modular helium reactor (MHR), which can be used to produce electricity as well as hydrogen, can operate at high temperatures of approximately 850°C. Advanced high temperature reactors (AHTR) have been proposed to address the requirements specific to high temperature hydrogen production. However, an AHTR has not been built yet. Another reactor technology that can meet the requirements of high temperature hydrogen production is a Secure Transportable Autonomous Reactor (STAR), which is a fast neutron spectrum modular sized reactor. It is based on a Russian submarine reactor technology that was demonstrated at temperatures of around 500°C. The coolant of the reactor is liquid lead and it has a reactor core outlet temperature of around 850°C [23].

The Japan Atomic Energy Research Institute has been conducting research and development on High Temperature Gas-cooled Reactors (HTGR), and on hydrogen production using HTGR. The reactor technology has been developed using a High Temperature Test Reactor (HTTR) installed at the Oarai site of JAERI. The reactor reached its full power output of 30 MW in 2001. The reactor outlet helium temperature was demonstrated to reach 950°C in 2004 [21]. The integration of the S-I cycle and the HTTR is still under research and development. The aim is to develop this technology for safe and economical operation. The research on integrating the cycle and the nuclear reactor requires the technology to be safe, in terms of safety against explosion, safety against any radioactive material release, and safe control to prevent any thermal disturbance from the hydrogen production plant to the reactor.

Xinxin et al. [24] have demonstrated experimentally the process of hydrogen production by the S-I cycle. The results obtained from the lab scale experiment confirmed the feasibility of the closed loop operation for recycling all of the reactants except water, hydrogen and oxygen. A membrane technology to increase the decomposition efficiency was developed. This was shown to be a better method to convert the HI acid. The conversion rates of HI that were attained by one pass were 90%, using the membrane technology, compared to an equilibrium rate of about 20%.

### 2.2.5 Copper-Chlorine Cycle

The copper-chlorine (Cu-Cl) cycle has been identified by AECL as the most promising cycle for thermochemical hydrogen production with the next generation of CANDU Super Critical Water Reactors (SCWR). It has the advantage of having low operating temperatures and potentially lower cost material, when compared to other thermochemical cycles, that are developed in other countries around the world [25].

AECL and the Argonne National Laboratory in the U.S. have been collaborating to develop the Cu-Cl cycle for hydrogen production using nuclear energy or waste heat from nuclear plants [26]. The Cu-Cl cycle requires heat at temperatures up to 500°C. This makes it feasible for integration with SCWR. The cycle is composed of four chemical reactions and one electrochemical process. The reaction steps of the cycle are shown in Table 2.1.

Table 2.1 Reaction steps in the Cu-Cl cycle.

| Step | Reaction | Temperature (°C) |
|---|---|---|
| 1 | $2Cu(s) + 2HCl(g) \rightarrow 2CuCl(l) + H_2(g)$ | 450 |
| 2 | $2CuCl(s) + 2CuCl(aq) \rightarrow CuCl_2(aq) + Cu(s)$ | 25 |
| 3 | $CuCl_2(aq) \rightarrow CuCl_2(s)$ | > 100 |
| 4 | $2CuCl_2(s) + H_2O(g) \rightarrow CuO*CuCl_2(s) + 2HCl(g)$ | 400 |
| 5 | $CuO*CuCl_2(s) \rightarrow 2CuCl(l) + 1/2O_2(g)$ | 500 |

Water, heat and electricity are the only inputs to the cycle. The copper and chlorine compounds are recycled within the cycle. The net reaction of the cycle is the production of hydrogen and oxygen gases by splitting water molecules. The first step in the cycle is the HCl production step, step 4 in Table 2.1. In this step, cupric chloride reacts with water to produce HCl gas and a $CuO*CuCl_2$ compound. This reaction is an endothermic reaction that occurs at temperatures around 400°C in a fluidized bed. The $CuO*CuCl_2$ compound moves to the next step, which is the oxygen production step, step 5 in Table 2.1. The HCl gas moves to the hydrogen production step, step 1 in Table 2.1. In the oxygen production step, oxygen is released from the $CuO*CuCl_2$ compound by adding heat, and the reaction proceeds at temperatures of

around 500°C. The products of the oxygen production step are oxygen gas and molten CuCl. The molten CuCl moves to the copper production step, step 2 in Table 2.1, to produce solid copper particles, which are needed by the hydrogen production step. The copper production reaction is carried out at low temperatures, lower than 100°C, and achieved by supplying electricity to the reaction. In the hydrogen production step, solid copper particles react with HCl gas to produce hydrogen at temperatures of around 400°C. The hydrogen production reaction is an exothermic reaction. The final step in the cycle is the drying step, which is step 3 in Table 2.1. The purpose of this step is to dry the $CuCl_2$ particles and produce solid $CuCl_2$ that is needed in the HCl production step. By carrying out the above mentioned steps, the cycle completes itself. Figure 2.2 shows a conceptual schematic of the Cu-Cl cycle.

Wang et al. [8] have examined the heat requirements of different steps in the Cu-Cl cycle. The primary goal of the study was to match the heat requirements of various steps within the cycle, in order to maximize the operational efficiency of the cycle. Matching the heat requirements was achieved by recovering heat from the products of the high temperature reactions, and using it to supply the heat requirements of other lower temperature reactions.

Naterer et al. [10] examined the performance of the Cu-Cl cycle under different operating conditions. The conditions included no heat recovery, full heat recovery, and partial heat recovery within the cycle, with and without losses to the surroundings. It was found that the cycle's practical efficiency without any heat recovery is 46%. The cycle efficiency for other cases varied between 37%, when considering 20% losses to the surroundings, and no heat recovery at all, up to a limiting value of 74%, when 100% of the heat was recovered and 0% losses to the surroundings were assumed. The study also examined the thermal design of the

oxygen production reactor, since it is a key process to split the water molecules. Solutions to the major thermal design challenges of the oxygen reactor were also given.

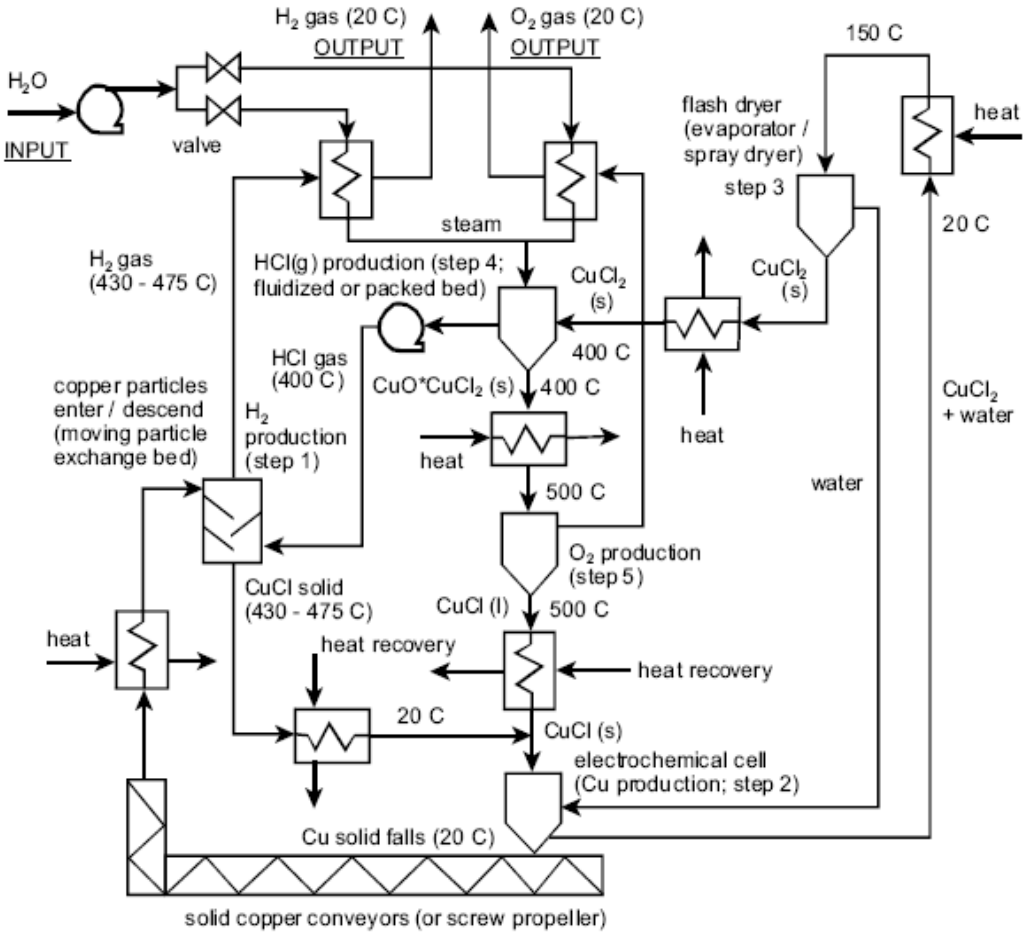


Figure 2.2 Conceptual schematic of a Cu-Cl cycle [27].

Naterer et al. [25] have also examined the evaporative drying process of the aqueous cupric chloride ($CuCl_2$) in the Cu-Cl cycle. Analytical solutions for the cupric chloride spraying and drying processes were developed, including empirical correlations for heat and mass transfer for a single droplet of an aqueous cupric

chloride solution. The models can be used to predict the ideal drying conditions, for utilizing low temperature waste heat from power plants.

Orhan et al. [28] analyzed a Cu-Cl pilot plant economically. The analysis took into account different components of the cost, such as energy, operation and maintenance costs. The total capital investment and total cost of the Cu-Cl pilot plant were determined through a scaling method, and related to costs of a commercial S-I plant. It was found that the fixed capital investment and the product cost of a Cu-Cl pilot plant, with a production capacity of 5 tons per day, were US$27.5 million and US$4.7 million respectively.

Most of the current research on hydrogen production focused on utilizing nuclear energy. Botterud et al. [29] developed a financial model that is based on a real options theory of assessing the profitability of four different nuclear hydrogen production technologies. The research showed a significant value of switching the plant output between electricity and hydrogen.

Kimura et al. [30] investigated the feasibility of hydrogen production from biomass by nuclear heat. A significantly better efficiency was obtained from this process, compared to other reaction processes such as electrolysis from a renewable source. However, it involves a small amount of carbon dioxide emission.

Torjman et al. [31] have assessed the production of hydrogen from nuclear energy, economically and environmentally. It was proposed that a complete nuclear-electro-hydrogen energy system can supply the energy requirements of a medium size city with a population of 500,000 people.

Verfondern et al. [32] have shown the technical feasibility of using HTGR in combination with a coal gasification process. The research described German projects on a prototype nuclear process heat system.

Horie et al. [33] presented a method to produce hydrogen synergistically through steam reforming of fossil fuels and nuclear heat. The steam reforming process used a membrane type reformer and recalculated the reaction products in a closed loop. The study compared different synergetic hydrogen production processes and found that the suggested method was the most profitable. The suggested method leads to lower carbon dioxide emissions, has a small size, and produces high purity hydrogen. The heat supplied from the nuclear reactor to the process must be at a temperature of 550°C.

## 2.3 Hydrogen Storage

The problem of hydrogen storage has attracted the efforts of many researchers. The aim is to find an inexpensive and efficient method to store hydrogen, so that it can be handled just like any other known fuel and used in everyday applications.

Schlapbach et al. [34] have categorized hydrogen storage into three main methods: compressed gaseous hydrogen storage, liquid hydrogen storage, and hydrogen storage as hydrides. Hydrogen is available commercially in pressurized tanks at pressures of around 20 MPa. However, these tanks cannot hold enough hydrogen to power a vehicle for an acceptable range of around 300 miles. In order for the storage cylinders to hold a larger amount of hydrogen, the storage pressure has to be increased, but this will increase the weight and material cost of the tank.

Cumalioglu et al. [35] outlined the primary requirements of a hydrogen storage tank to include low density, non-reactive with hydrogen, high tensile strength, and low diffusivity. Other properties such as the permeability, fatigue strength, and aging are important for material selection criteria of hydrogen storage tanks.

Kandavel et al. [36] investigated hydrogen storage improvements through the use of Ti1.1CrMn AB2-type Laves phase alloys, for low and high temperature applications ranging from -30 to 80°C. It was found that the hydrogen storage properties were improved by substituting Ti atoms with Zr atoms. The increase in Zr content decreases the hydrogen pressure absorption plateau, and increases the absorption kinetics. A noticeable increase in hydrogen storage capacity was noted for the TI1.1CrMn and (Ti0.9Zr0.1Mn)1.1CrMn alloys to be 1.9 – 2.2 wt%, respectively.

Damle et al. [37] gave a brief description of liquid and hydride hydrogen storage. The main benefit of liquid hydrogen storage is the increase in its volumetric density at relatively low pressures. This means that larger quantities of hydrogen can be stored in the same tank volume. Hydrogen can be stored as a hydride in two categories: metal hydrides and chemical hydrides. In both categories, hydrogen is stored as a compound. Hydrogen storage as a metal hydride has the benefit of being able to be released onboard reversibly at low temperatures and pressures. However, metal hydrides have large weights.

## 2.4 Droplet Motion and Heat Transfer

Droplet motion and heat transfer are key processes in the heat recovery of molten CuCl. Understanding the fluid flow around a sphere is the first step to calculate the heat transfer rate from droplets. In a convection heat transfer problem, the first step towards finding the convection heat transfer coefficient is to find the velocity gradients around the object of interest, from the governing momentum equation, in order to find the velocity distribution. Then these velocities are used to solve the governing energy equation, which in turn gives the temperature distribution or heat transfer rate. Much past work has been done on the motion and heat transfer

characteristics of droplets. Onuki et al. [38] examined spherical droplet motions that are changing phase in fluids with small temperature gradients. The droplet motion was studied by solving the linearized hydrodynamic equations that govern the fluid flow. The study showed that the velocity and temperature gradients are strongly influenced by the phase transition process of the droplet at the surface. Latent heat released or absorbed at the interface drastically changes the hydrodynamic flow around the droplet, which results in a nearly homogenous temperature inside the droplet.

De Villeneuve et al. [39] experimentally studied the approach of similarly sized droplets and rigid spheres to a colloidal gas-liquid interface. It was concluded that liquid droplets approach the interface slightly faster than rigid spheres, and the approach velocities converge close to the interface.

Masoudi et al. [40] investigated the unsteady three-dimensional interaction of an initially cylindrical vortex tube with a droplet in a uniform stream. The investigation was carried out by numerically solving the Navier-Stokes equations. A correlation of the effect of the advecting vortex on the droplet heating was developed. The correlation complements other models of droplet heating in axisymmetric flows that occur in the absence of an advecting vortex.

Quan et al. [41] simulated a liquid spherical droplet that was impulsively accelerated by a gaseous flow, to investigate the drag force and deformation of the droplet. The dynamics of the droplet was found by solving the incompressible Navier-Stokes equations, using a finite volume staggered mesh, coupled with a moving mesh interface tracking scheme. It was found that the droplet deforms as it accelerates. The deformation factor of the droplet was found to be 0.2. The drag coefficient is higher

than typical steady-state drag coefficients of rigid spheres at the same Reynolds number.

Ni et al. [42] simulated a droplet falling in a different background liquid. The complete Navier-Stokes equations were solved using a projection method, coupled with a level set method. The study showed the effect of the inertial force on the deformation and oscillatory motion of the droplet, by changing the Reynolds number for several Weber numbers.

Feng et al. [43] numerically studied the transient heat transfer from a sphere at high Reynolds and Peclet numbers. The governing equations of the problem were made dimensionless, then were solved using the stream function-vorticity formulation. The simulation results were compared to experimental data to validate the solution method. Good agreement was found between them. The study concluded that there is a strong dependence of the rate of heat transfer on Reynolds number, when the Peclet and Reynolds numbers are larger than one.

Feng et al. [44] also numerically studied the heat and mass transfer phenomena for a viscous sphere. The steady state Navier-Stokes and energy equations for the flow fields inside and outside the viscous sphere, in a fluid of different properties, were solved numerically for Reynolds numbers ranging from 1 to 500, and Peclet numbers ranging from 1 to 1000. The aim of the study was to find the Nusselt and Sherwood numbers, in order to find the heat and mass transfer coefficients. Both numbers were given in a correlation form by the authors. The study found that the Reynolds, Peclet, Prandtl, and Schmidt numbers, along with the viscosity ratio, have an important role on the rate of heat and mass transfer from a viscous sphere.

Kartushinskii et al. [45] modeled a gas-particle flow and simulated it. The model used an Eulerian description of the dispersed phase. A comparison between the

results of the model, and experimental distribution of the turbulence intensity in single and two phase flows, showed that the model accurately describes the effect of the particles on the carrier-gas turbulence. The model can be used to describe the specific features of the particle mass concentration distributions, in upward and downward pipe flows for various particle sizes, physical densities, and mass concentrations.

Feng et al. [46] developed a heat transfer equation that describes the unsteady heat transfer from a sphere in viscous / conducting fluids at various Biot numbers. The heat transfer process had two characteristic times; one for the diffusion of heat inside the sphere, and the other for diffusion of heat in the external fluid. It was found that the complete form of the energy equation was formulated for a small sphere, even at very small Peclet numbers.

Kadja et al. [47] modeled and simulated the heat, mass and momentum transfer between a slurry droplet and gas flow. No validation of the model was possible due to the lack of experimental data. However, the model showed that the most important factor in slurry drying is the ambient temperature, which agrees with other data in the literature [47].

Whitaker [48] collected previous heat transfer data and analyzed them to develop new correlations for finding the Nusselt number in various heat transfer problems. The correlations have a wide application range. They are relatively easy to use and have satisfactory accuracy for most design calculations. The correlations describe forced convection heat transfer for flow in pipes, past flat plates, single cylinders, single spheres, and flow in packed beds and tube bundles.

Levi et al. [49] analyzed the solidification of undercooled spherical droplets with a discrete melting temperature, using a Newtonian and a non-Newtonian model. The mathematical formulation and solution methodology were developed for

simulating the solidification process in an undercooled droplet, from a single nucleation event occurring at its surface. The simulation was conducted for aluminum droplets. The results showed that the Newtonian model provided a good dimensionless enthalpy-temperature diagram that describes the thermal history of the droplet. The non-Newtonian model showed that departures from the Newtonian model could occur at low Biot numbers, as low as $10^{-4}$.

Mitrovic et al. [50] investigated the temperature distribution of a fluid in a direct contact heat exchanger. The heat exchanger was a column with two immiscible fluids in countercurrent flow. None of the fluids underwent a phase change, so only sensible heat transfer was considered. Equations for the mean temperature of the fluids were derived analytically by integration of the one dimensional energy equation. The computed results were compared to experimental results, which showed satisfactory agreement.

Shimizu et al. [51] developed a heat exchanger to be used with particles or granular material and a gas. The primary goal behind the design of the heat exchanger was to recover the heat carried by the particles. The heat exchanger made use of a swirling gas flow, similar to cyclone separators, but with a downward axial velocity instead of an upward axial velocity. The heat exchanger was built based on numerical simulations, and tested experimentally. The heat exchange performance was found to be poor due to insufficient radial dispersion of the particles. Even when sufficient radial dispersion was obtained, the outlet gas temperature was not much higher than the outlet particle temperature.

Daggupati et al. [52] examined low-temperature heat transfer and evaporative drying of molten salt droplets in a thermochemical copper-chlorine cycle for hydrogen production. Due to the low temperature requirements of the Cu-Cl cycle, it

can make use of waste heat from thermal power plants. This leads to a reduction in thermal pollution, and better overall efficiency of power plants. It was shown that the Cu-Cl cycle is a promising alternative to the S-I cycle, due to its lower operating temperatures, lower material cost and waste heat utilization from any nuclear or industrial sources.

## 2.5 Heat Recovery

Heat recovery systems and methods have attracted the efforts of researchers due to their ability to increase the overall system performance. Much work has been performed on recovering heat within systems that operate over small and large temperature ranges. Recovering heat in the metal industry has great importance. Errera et al. [53] have analyzed a coke dry quenching (CDQ) unit thermodynamically, using the first and second laws. The analysis was performed for a unit under normal operating conditions. Data were measured experimentally on site. Expressions for finding the coke specific heat, enthalpy, entropy, physical and chemical exergies, particulate material formation indices, and the coke mass loss through chemical reactions, were developed. The analysis was extended further to a coke wet quenching (CWQ) unit to compare between the two processes. The results obtained through the analysis were compared to past literature, and were found to be consistent. It was also shown that the CDQ process is thermodynamically better than the CWQ process, by finding the destroyed exergy in both. The CDQ process had almost half the destroyed exergy of the CWQ process.

Zarrinehkafsh et al. [54] developed a mathematical model of heat transfer in fixed bed regenerators. A simulation of convective and conductive heat transfer within a fixed bed, made up of ceramic balls, was preformed. Experiments were also

conducted for a fixed bed, to compare both results. It was found that there is a small difference between the calculated values of effectiveness from simulation and experimental results. This was attributed to the errors associated with experimental measurements, and neglecting the radiation heat transfer mechanism at high temperatures.

Caputo et al. [55] performed real-time analysis of moving cooling beds that are used in heat recovery systems. Unlike other studies found in the literature, the analysis assumed the heat transfer process to be transient, instead of steady-state. A model was developed based on two-dimensional and time-dependant convective-conductive heat transfer. The model was simulated for the operating conditions of the cooling section of an iron-ore sintering bed in the Ilva steelworks plant in Taranto, Italy. The results of the simulation were validated after comparisons with experimental results. The model was shown to be a powerful tool for the design of moving cooling beds, instead of assuming steady-state conditions. This will result in a much better performance of the beds, especially from an economical standpoint.

Nassab [56] analyzed the transient heat transfer characteristics of an obstructing porous layer. A high temperature flow of hot non-irradiating gas, flowing through homogenous porous media was studied. Heat recovery by this obstructing porous media was achieved by absorbing the irradiative heat flux emitted from it. A numerical simulation of the heat transfer process was carried out. It was found that the porous media operates very efficiently in the first period of operation, where it absorbs energy from the flow. Recovering the absorbed energy, by means of absorbing thermal radiation from the media, was found to be most efficient when the media had a large optical depth and small scattering coefficient. The analysis was

validated through comparisons with experimental data. This method of heat recovery is most suited for systems that operate in unsteady conditions.

Bisio et al. [57] reviewed energy recovery methods of industrial steel and iron plants by evaporative cooling techniques. It was found that the capital cost of waste energy recovery plants is considerably higher than fuel-fired boilers, including ancillary equipment and buildings. The lowest capital cost of evaporative energy recovery plants was for plants utilizing evaporative recovery with natural circulation of open hearth furnaces, followed by plants utilizing evaporative cooling with forced circulation hearth furnaces, and finally plants utilizing a combination of waste heat boilers and evaporative cooling in open hearth furnaces.

Skiepko et al. [58] modeled and simulated the effect of leakages on the heat transfer performance of a fixed matrix regenerator. The main sources of leakages were gas leakages due to pressure differences, and gas carryover leakages from hot to cold gases, or vice versa. It was found that the heat transfer performance decreased linearly with the amount and type of leakages in the system. The highest drop in the effectiveness was found to be caused by flow leaks in the housing of the regenerator, due to cracks.

Pasini et al. [59] investigated methods to recover energy from aircraft engines. The purpose of the study was to increase the operating efficiency of aircraft engines, since they usually operate in off design conditions, by recovering heat from the exit air stream. The analysis showed that recovering energy from the exit stream of an aircraft engine affects its thermodynamic performance. It also improves its operating characteristics by requiring a lower pressure ratio, and consequently lowering the levels of $NO_x$ emissions. The problem of constructing a heat exchanger to recover the heat from the aircraft engine still stands, and further theoretical analysis is required.

These past methods indicate a number of methods to analyze heat recovery and droplet dynamics. However, none are directly applicable to molten CuCl heat recovery in the present configuration of the Cu-Cl cycle. The next chapter will present a new formulation with these required capabilities.

# Chapter 3

## Fluid Flow and Heat Transfer Formulation

This chapter presents the processes and formulation used for solving the fluid flow and heat transfer problem. A description of the model and solution method are given.

### 3.1 Fluid Flow around Spheres

Fluid flow around spheres is often categorized into two flow regimes; low Reynolds number flows and high Reynolds number flows. Low Reynolds number flows are further categorized into two main flow types; creeping flows, which are categorized by the condition $Re << 1$, where the inertia of the fluid can be neglected, and small but finite Reynolds number flows, which are categorized by the condition $Re < 1$, where the inertia of the fluid is taken into account. In small Reynolds number flows, bubbles and droplets maintain a spherical shape, and the flow analysis for solid particles, spheres and spheroids are the same. Also, the flow around droplets is asymmetric only for small Reynolds number flows, when $Re << 1$ [60].

At high Reynolds numbers, $Re > 1$, the flow becomes distorted, and a wake is generated at the back of a droplet. The generated wake is initially steady, then it gets stronger with increasing Re. At very high Reynolds numbers, the wake becomes unsteady and very strong, which results in shedding of vortices. High Reynolds number flows around solid spheres have six different regimes [60]:

1- Attached flow (1 < Re < 20): the flow remains attached to the droplet surface and separation does not occur in this flow regime. The generated wake behind the droplet is weak and steady. Figure 3.1 shows the flow streamlines and vorticity contours for a flow with a Reynolds number equal to 1. The streamlines are shown on the top half of the figure, and the vorticity contours on the bottom half.

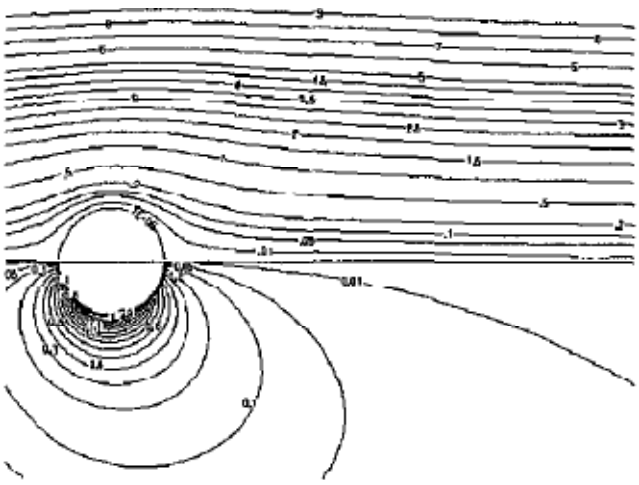

Figure 3.1 Streamlines and vorticity contours for a flow past a solid spherical droplet at Re = 1 [60].

2- Steady-state wake (20 < Re < 130): at the beginning of this flow regime, a weak circulation region is attached to the back of the droplet. As Re increases, the wake becomes stronger, its width and length increase, and its point of attachment moves forward on the surface of the droplet. Figure 3.2 shows the streamlines and vorticity contours for a flow with a Reynolds numbers equal to 100. The streamlines are shown on the top half of the figure, and the vorticity contours on the bottom half.

3- Unsteady wake in laminar flow (130 < Re < 270): at the beginning of this flow regime, a weak, long-period oscillation at the tip of the wake occurs. Oscillations increase with increasing Re, but the wake remains attached to the droplet. In this flow regime, the viscous effects have a small role on the value of the drag coefficient. Most of the generated drag is due to the pressure difference between two sides of the droplet. The flow outside of the wake remains laminar throughout this flow regime.

4- Vortex shedding (270 < Re < 6,000): pockets of vorticity begin to be shed away from the tip of the droplet in this flow regime. This influences the flow velocity and its fluctuations at far fields. The separation point of the flow moves forward on the droplet's surface, reaching a point on the droplet that corresponds to an angle measured from the forward axis of the sphere of 83°. Figure 3.3 shows the streamlines and vorticity contours for a flow with a Reynolds number equal to 500. The streamlines are shown on the top half of the figure, and the vorticity contours on the bottom half.

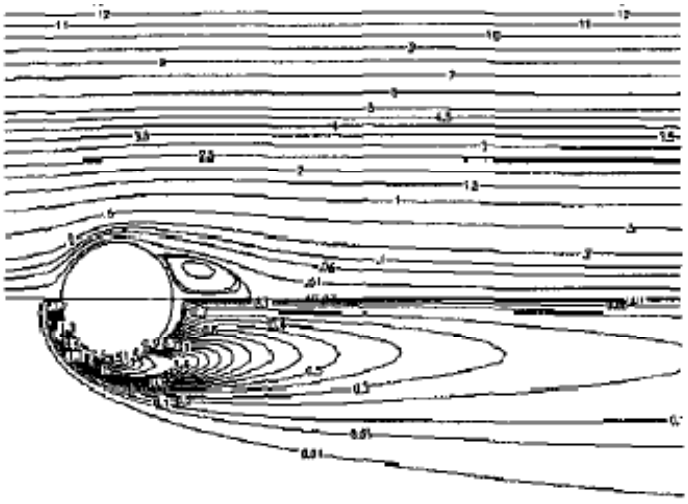

Figure 3.2 Streamlines and vorticity contours for a flow past a solid spherical droplet at Re = 100 [60].

5- Unsteady boundary layer separation (6,000 < Re < 300,000): at the beginning of this flow regime, which is usually called the "lower critical Reynolds number", the separation point at the droplet surface starts rotating around the droplet in a frequency equal to the vortex shedding frequency. The wake behind the droplet does not reach a turbulent stage, and the value of the drag coefficient reaches an almost constant value throughout this flow regime.

6- Transition and supercritical flow (Re > 300,000): the wake becomes turbulent in this flow regime. The transition to a turbulent wake starts at Re = $2 \times 10^5$ and it is completed at Re = $3.7 \times 10^5$. However, the critical point of transition is usually accepted at Re = $3 \times 10^5$. The point of separation moves downstream of the droplet, from an angle of 83° to 120°, and remains constant afterwards. The free shear layer in the flow becomes turbulent and attached to the surface of the droplet, which is what causes a sharp reduction in the value of the drag coefficient.

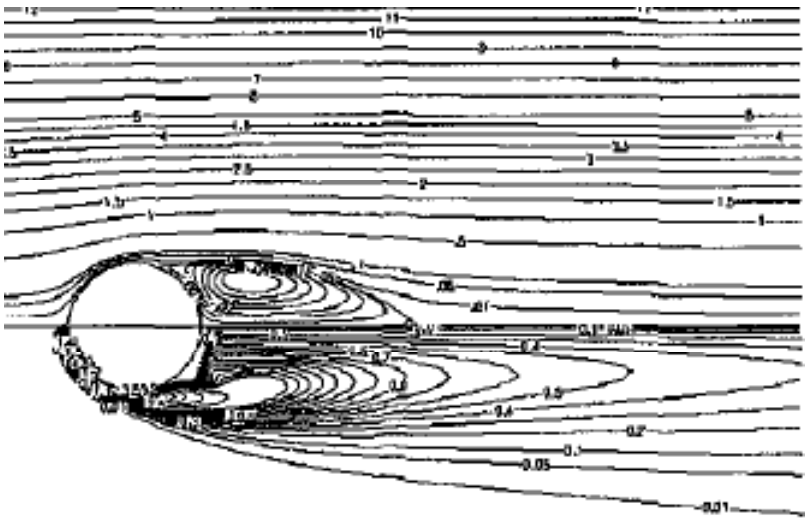

Figure 3.3 Streamlines and vorticity contours for a flow past a solid spherical droplet at Re = 500 [60].

Flow around liquid droplets has the same characteristics as that of solid droplets. However, at high Reynolds numbers, the shear stresses acting on the droplet's surface lead to a significant shape distortion that might lead to break-up of the droplet. Most droplets and bubbles break up before reaching a Reynolds number of 1,000 [60]. Therefore, the first four flow regimes around a solid droplet have importance for the study of flow around liquid droplets. The main differences between flow around liquid and solid droplets are given as follows:

1- Internal circulations within liquid droplets delay the formation of the wakes by delaying the boundary layer separation. They also cause the length of the wake to be slightly shorter.
2- Two symmetric internal weak wakes appear at the back of liquid droplets at high Reynolds numbers. These cause a flow reversal at the rear of the droplet, so the velocity vector points in the positive direction for a short distance.

Determining the drag coefficient has importance when analyzing flows around droplets. Many experimental studies have been conducted to develop empirical correlations for the drag coefficient at different Reynolds numbers. The "standard drag curve" was observed between values of Reynolds numbers ranging between 0 – 0.1, where the drag exhibits a Stokesian behavior for solid spheres. Then in the range of $0.1 < Re < 0.4$, the drag force follows the Oseen law. Then it decreases monotonically with increasing Re, while diverging from both Stokes and Oseen expressions. As Re increases, viscous effects become less significant, and so the drag curve flattens. In this range, the main source of drag is pressure drag. The drag coefficient stays almost constant, over the range of Reynolds number between 1,000

to $2 \times 10^5$. At a value of approximately $Re = 3.7 \times 10^5$, the drag coefficient drops drastically. This is due to flow transition to turbulence. Then the drag coefficient increases slightly with increasing Reynolds number, after the transition to turbulent flow [60].

For analyzing flows over liquid droplets or spheres, the shape deformation has to be taken into account when computing the drag force. It is usually accepted in practice that spheroidal droplets may be assumed spherical, when the values of the length of their two principal axes are within 5%. The existence of internal flows within liquid droplets affects the external flow. Values of the vorticity gradients around liquid droplets are significantly lower than for a solid particle. As a result, the drag coefficient for a liquid droplet is lower than that of a solid droplet. An important parameter that affects the drag coefficient for liquid droplets is the viscosity ratio, which is the ratio of the droplet's viscosity to the fluid viscosity. Droplets with high viscosity ratios behave like solid particles, just as the case of liquid metal droplets [60].

Many correlations for determining the drag coefficient as a function of Reynolds number can be found in past work [60,61]. The correlations are valid for specified Reynolds number ranges, depending on the flow regime studied, and there are different correlations for liquid and solid droplets.

## 3.2 Velocity Distribution

There are two main velocity distributions that need to be found, in order to find the velocity distribution, and solve the heat transfer problem for droplets. These velocity distributions are for the droplet and fluid.

### 3.2.1 Droplet Velocity Distribution

Consider droplets released from the top of a drop tower, which fall under gravity, and transfer heat to the surrounding gas stream. When the droplet enters the heat exchanger from the top, its velocity starts from a value of near zero, then increases until it reaches a value where the upward forces equal the downward forces acting on the droplet. This value is called the terminal velocity. Figure 3.4 shows a free body diagram of the forces acting on a droplet that is freely falling in an air up flow. Three main forces act on the droplet; the droplet's weight, drag force and buoyancy force. Applying a force balance on the droplet will result in the following equation, assuming positive direction downwards.

$$F_R = F_W - F_D - F_B \tag{3.1}$$

where $F_R$ is the resultant force, $F_W$ is the weight force, $F_D$ is the drag force, and $F_B$ is the buoyancy force. The weight force is caused by gravity. It can be found using the following equation:

$$F_W = m_d\, g \tag{3.2}$$

where $g$ is the gravitational acceleration. The mass of the droplet can be found by multiplying its volume by the droplet's density as follows:

$$m_d = v_d\, \rho_d \tag{3.3}$$

where the droplet volume can be found by:

$$v_d = \frac{4}{3}\pi {r_d}^3 \tag{3.4}$$

The buoyancy force is generated due to the density difference between the droplet and the flowing fluid around it. It can be found by the following equation:

$$F_B = m_d\, g\, (\frac{\rho_f}{\rho_d}) \tag{3.5}$$

Since the density ratio of the fluid to the droplet is very low, this force was neglected in the analysis. The ratio was always less than 0.0003 throughout the heat exchanger, so the generated buoyancy force was less than 0.03% of the droplet's weight, which justifies the assumption of neglecting it.

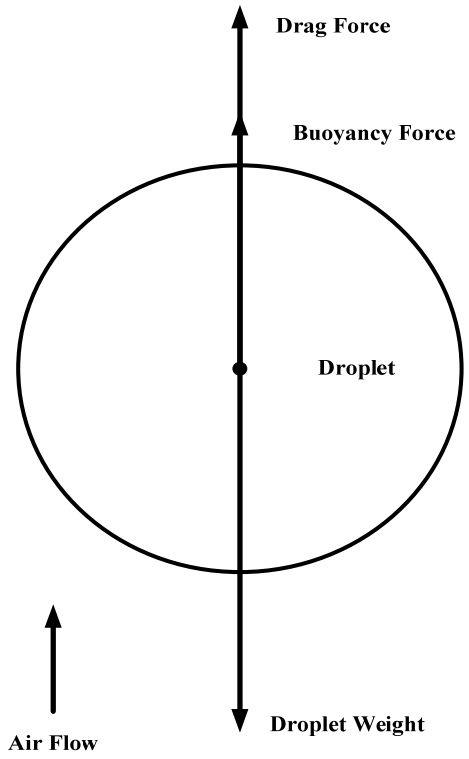


Figure 3.4 Free body diagram of the forces acting on a droplet.

The drag force can be found by the following equation:

$$F_D = \frac{1}{2}\,\rho_f\,A_c\,C_D\,{V_T}^2 \tag{3.6}$$

where $A_c$ is the cross-sectional area of the droplet, which can be found by:

$$A_c = \pi\,{r_d}^2 \tag{3.7}$$

Also, $V_T$ is the relative velocity, which is the sum of the droplet ($V_d$) and fluid ($V_f$) velocities, as expressed in the following equation:

$$V_T = V_d + V_f \tag{3.8}$$

where $C_D$ is the drag coefficient for the droplet, which can be found by the following correlation [60]. This is valid over the Re range between 1 – 800, which is the range of interest for the droplet and fluid motions within the heat exchanger:

$$C_D = \frac{24}{Re}(1 + 0.15\,Re^{0.687}) \tag{3.9}$$

Finally, the resultant force can be expressed by the following equation:

$$F_R = m_d\,a_d \tag{3.10}$$

where $a_d$ is the resultant droplet acceleration. Substituting equations (3.2), (3.6) and (3.10) into equation (3.1), after neglecting the buoyant force, the droplet's resultant acceleration can be expressed as:

$$a_d = g - \left(\frac{C_D \, \rho_f \, A_c \, {V_T}^2}{2 \, m_d}\right) \tag{3.11}$$

Then the droplet velocity ($V_d$) can be found at any height in the heat exchanger by the following summation, assuming that $a_d$ has a constant value throughout every element:

$$V_{d,e}(H) = \sqrt{{V_{d,i}}^2 + \sum_{h=0}^{h=M} 2 \, a_d \, H} \tag{3.12}$$

where $H$ is the height of each element, $M$ is the number of elements that correspond to the required height, and $V_{d,i}$ is the inlet velocity of the droplet at the top of the tower. This was assumed to have small finite values throughout the study. The total velocity ($V_T$) must be known to determine the droplet's velocity at any height. Therefore, the analysis of the fluid flow, in order to determine values for $V_T$, is required.

### 3.2.2 Fluid Velocity Distribution

The cooling fluid enters the heat exchanger from the bottom. It initially has a uniform velocity, called the fluid inlet velocity ($V_{f,i}$). As the fluid moves upwards, its temperature increases, due to heat transfer from the droplets to the fluid. The fluid will expand as its temperature increases, and because the fluid is only allowed to

expand in the upward axial direction, its velocity will increase. This increase in the fluid's velocity is called the fluid expansion velocity ($V_{f,exp}$).

The fluid inlet velocity can be determined using the following equation:

$$V_{f,i} = \frac{\dot{m}_f}{\rho_{f,i} A_f} \tag{3.13}$$

where $\dot{m}_f$ is the mass flow rate of the fluid, $\rho_{f,i}$ is the density of the fluid at the inlet conditions, and $A_f$ is the cross sectional area of the heat exchanger. The heat exchanger was assumed to have a cylindrical shape, so $A_f$ can be found using the following expression:

$$A_f = \pi {r_f}^2 \tag{3.14}$$

The fluid expansion velocity, $V_{f,exp}$, can be found by knowing the change in the volume flow rate and dividing it by the cross sectional area of the heat exchanger. This is expressed as:

$$V_{f,exp} = \frac{(\upsilon_{f,e} - \upsilon_{f,i})\, \dot{m}_f}{A_f} \tag{3.15}$$

where $\upsilon_{f,e}$ and $\upsilon_{f,i}$ are the specific volumes of the fluid at the exit and inlet conditions respectively.

Since the fluid flow distribution is known, the relative velocity ($V_T$) can be expressed as:

$$V_T = V_{f,i} + V_{f,exp} + V_d \quad (3.16)$$

where the summation of the fluid inlet velocity ($V_{f,i}$) and the fluid expansion velocity ($V_{f,exp}$) is the fluid velocity $V_f$, which is expressed as:

$$V_f = V_{f,i} + V_{f,exp} \quad (3.17)$$

The fluid inlet velocity is constant throughout the heat exchanger height, but the fluid expansion velocity and the droplet velocity are not. Therefore, the total velocity varies throughout the height of the heat exchanger. The fluid expansion velocity and the droplet velocity are also functions of temperature, since temperature is the driving force for the fluid expansion, which affects the value of the drag coefficient, and therefore affects the droplet's velocity. The total velocity is also needed in the heat transfer analysis, since it is needed to find Re throughout the heat exchanger height, in order to find Nu.

## 3.3 Direct Contact Heat Transfer

Direct contact heat transfer occurs whenever two substances at different temperatures contact each other physically. This physical interaction accomplishes very efficient heat transfer, due to the low thermal resistance associated with the process. Direct physical interaction also allows for mass transfer to take place, which in some cases is desirable, for example in cooling towers [61]. Cost is often more favorable for direct contact heat exchangers than conventional heat exchangers, which incorporate a barrier wall between the two substances.

Direct contact heat transfer is a field with a wide range of potential applications. However, it has a very limited use in practical applications, such as open feed water heaters and cooling towers. This is mainly due to the lack of knowledge of how this type of heat exchanger can be designed [61].

Heat transfer from the continuous phase to the droplet, or vice versa, is a complicated process. It involves convection heat transfer, and potentially radiation heat transfer, if temperatures are high enough, complex variations in different parameters, such as velocity, droplet diameter, complex droplet interactions, if the density of droplets is high, and so forth. Limited knowledge is available on convective heat transfer from molten salt droplets. Some correlations for determining Nu were found in [60,61]. The same applies in the case of heat transfer processes within droplets, as little work is available there too. Some correlations can also be found in [60,61] for analyzing heat transfer processes within droplets.

Spray columns are one of the basic designs of direct contact heat exchangers. They are used to transfer heat from a dispersed phase to a continuous phase, or vice versa. Other types of columns used as direct contact heat exchangers are baffled columns and packed columns. Figure 3.5 shows a schematic of a spray column. This type of configuration will be analyzed for the heat recovery from molten CuCl.

Three approaches exist for analyzing spray columns. The first approach is analogous to the design and analysis of conventional heat exchangers, based on the Log Mean Temperature Difference (LMTD) and Number of Transfer Units (NTU) methods. The second approach is called a global treatment approach, and the third is called a differential treatment approach [61]. The first and second approaches are general analysis approaches that can predict the required dimensions of the spray column, without information on the details of the variations of the different

parameters throughout the column. The third approach provides detailed behavior of the different parameters throughout the column. It requires dividing the column into discreet zones, then solving the fluid flow and heat transfer equations, and mass transfer if applicable, as governing equations throughout the column.

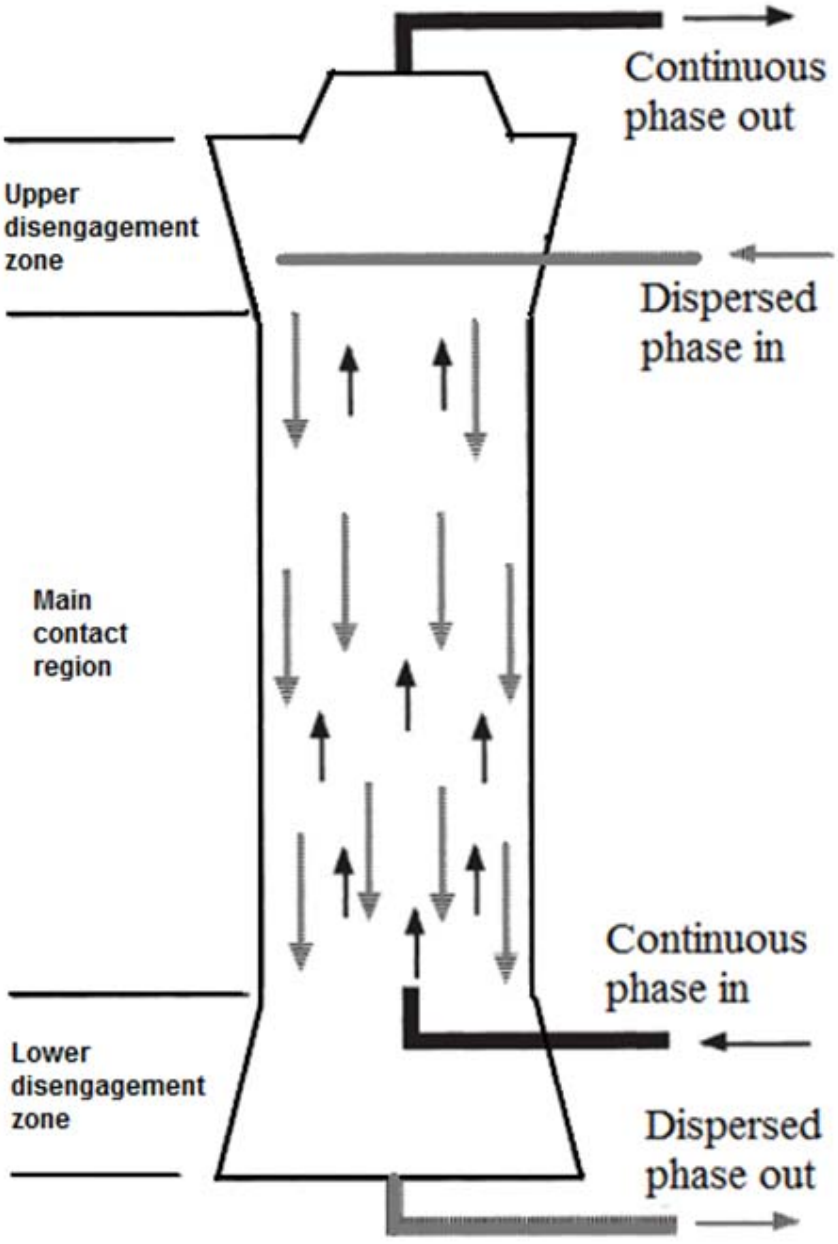


Figure 3.5 Schematic of a spray column [61].

### 3.4 Temperature Distribution

The temperature of the droplet will be assumed uniform throughout the heat exchanger height, i.e., assume lumped capacitance of the droplet so that internal temperature gradients within the droplet can be neglected. This means that the Biot number of the droplet must be less than 0.1. Further descriptions on maintaining the Biot number below 0.1 will be given in later sections. This condition can be expressed as:

$$Bi = \frac{h\, l_c}{k_d} < 0.1 \tag{3.18}$$

where $h$ is the convective heat transfer coefficient, $k_d$ is the droplet's thermal conductivity, and $l_c$ is the droplet's characteristic length. For spherical droplets, $l_c$ can be expressed as:

$$l_c = \frac{r_d}{3} \tag{3.19}$$

In order to find the convection heat transfer coefficient ($h$), the following correlation by Whitaker [48] can be used to find the average Nu from a sphere:

$$\overline{Nu_d} = 2 + \left(0.4\, {Re_d}^{0.5} + \ 0.06\, {Re_d}^{2/3}\right) {Pr_f}^{0.4} \left(\frac{\mu_f}{\mu_{f,s}}\right)^{0.25} \tag{3.20}$$

where $Re_d$ is the Reynolds number based on the droplet diameter, $Pr_f$ is the Prandtl number of the fluid, and $\mu_f$ and $\mu_{f,s}$ are the fluid dynamic viscosities. All properties are evaluated at the free stream temperature, except for $\mu_{f,s}$, which is evaluated at the

droplet's temperature. This correlation has an uncertainty of ± 30% at the very worst, and is valid over the following conditions:

$$3.5 \leq Re_d \leq 7.6 \times 10^4 \tag{3.21}$$

$$0.71 \leq Pr_f \leq 380 \tag{3.22}$$

$$1 \leq \frac{\mu_f}{\mu_{f,s}} \leq 3.2 \tag{3.23}$$

The Reynolds number can be found by the following expression:

$$Re_d = \frac{V_T D_d \rho_f}{\mu_f} \tag{3.24}$$

The Prandtl number can be found by the following expression:

$$Pr_f = \frac{C_{p\,f}\,\mu_f}{k_f} \tag{3.25}$$

where $C_{p\,f}$ and $k_f$ are the fluid's specific heat at constant pressure and thermal conductivity, respectively.

When $\overline{Nu_d}$ is found, the average convection heat transfer coefficient for the droplet ($\bar{h}$) can be found by the following equation:

$$\bar{h} = \frac{\overline{Nu_d}\,k_f}{D_d} \tag{3.26}$$

To find the temperature distribution, the convection heat transfer rate must be found, then the temperature change for both the fluid and the droplet can be found by applying a energy balance. The convection heat transfer rate can be expressed as:

$$\dot{Q}_{convection} = \bar{h}\, A_d \left(\frac{T_{d,i} + T_{d,e}}{2} - \frac{T_{f,i} + T_{f,e}}{2}\right) \tag{3.27}$$

where $A_d$ is the surface area of the droplet corresponding to the droplet mass flow rate, $T_{d,i}$ and $T_{d,e}$ are the temperatures of the droplet at the inlet and exit of each element respectively, and $T_{f,i}$ and $T_{f,e}$ are the temperatures of the fluid at the inlet and exit of each element, respectively. Also, $A_d$ can be found by the following equation:

$$A_d = \dot{N}_d\, 4\, \pi\, {r_d}^2 \tag{3.28}$$

The heat transfer rate from the droplet flow can be written as:

$$\dot{Q}_d = \dot{m}_d\, C_{p\,d}\, (T_{d,i} - T_{d,e}) \tag{3.29}$$

where $\dot{m}_d$ is the droplet mass flow rate, and $C_{p\,d}$ is the specific heat of the droplet at constant pressure. The mass flow rate, $\dot{m}_d$, can be expressed as:

$$\dot{m}_d = N_d\, m_d \tag{3.30}$$

where $\dot{N}_d$ is the droplet flow rate in droplets per second. The heat transfer rate to the fluid may be expressed as:

$$\dot{Q}_f = \dot{m}_f \, C_{p\,f} \, (T_{f,e} - T_{f,i}) \tag{3.31}$$

Assuming no losses in the heat transfer process will yield the following condition:

$$\dot{Q}_{convection} = \dot{Q}_d = \dot{Q}_f \tag{3.32}$$

By equating equations (3.29) and (3.31),

$$T_{d,i} = \frac{\dot{m}_f \, C_{p\,f}}{\dot{m}_d \, C_{p\,d}} \left(T_{f,e} - T_{f,i}\right) + T_{d,e} \tag{3.33}$$

From equation (3.31),

$$T_{f,e} = \frac{\dot{Q}_f}{\dot{m}_f \, C_{p\,f}} + T_{f,i} \tag{3.34}$$

After substituting equation (3.27) into (3.34), the exit temperature of the fluid becomes:

$$T_{f,e} = \frac{\frac{\bar{h}\,A_d}{2\,\dot{m}_f\,C_{p\,f}} T_{d,i} + \frac{\bar{h}\,A_d}{2\,\dot{m}_f\,C_{p\,f}} T_{d,e} + \left(1 - \frac{\bar{h}\,A_d}{2\,\dot{m}_f\,C_{p\,f}}\right) T_{f,i}}{\left(1 + \frac{\bar{h}\,A_d}{2\,\dot{m}_f\,C_{p\,f}}\right)} \tag{3.35}$$

There exist two heat transfer cases due to phase change of the droplet. In the first case, the temperature of the droplet is held constant during the phase change process, so $T_{d,i}$ and $T_{d,e}$ are equal. In the second case, the temperature of the droplet

changes between the inlet and exit, due to sensible heat loss. For the case of phase change, equation (3.35) simplifies to:

$$T_{f,e} = \frac{\frac{\bar{h}\,A_d}{\dot{m}_f\,C_{p\,f}}T_d + \left(1 - \frac{\bar{h}\,A_d}{2\,\dot{m}_f\,C_{p\,f}}\right)T_{f,i}}{\left(1 + \frac{\bar{h}\,A_d}{2\,\dot{m}_f\,C_{p\,f}}\right)} \tag{3.36}$$

This equation is used to determine the exit temperature of the fluid across each element during the phase change process of the droplet.

For the case of sensible heat transfer from the droplet, substituting equation (3.33) into equation (3.35) leads to:

$$T_{f,e} = \frac{\left(\frac{\bar{h}\,A_d}{\dot{m}_f\,C_{p\,f}}\right)T_{d,e} + \left(1 - \frac{\bar{h}\,A_d}{2\,\dot{m}_f\,C_{p\,f}} - \frac{\bar{h}\,A_d}{2\,\dot{m}_d\,C_{p\,d}}\right)T_{f,i}}{\left(1 + \frac{\bar{h}\,A_d}{2\,\dot{m}_f\,C_{p\,f}} - \frac{\bar{h}\,A_d}{2\,\dot{m}_d\,C_{p\,d}}\right)} \tag{3.37}$$

This equation is used to determine the exit temperature of the fluid across each element during sensible heat transfer processes.

## 3.5 Model Description

The model used for the design and analysis of the direct contact heat exchanger is based on the previous fluid flow and heat transfer equations. The fluid selected to recover heat from the molten CuCl is air. The known parameters for the model are the outlet temperature of the CuCl, the air inlet temperature, and the CuCl and air mass flow rates. The heat exchanger height was divided into $M$ elements, and each element had a height of 1 mm. The equations were solved throughout the heat exchanger height for every element, starting from the bottom and progressing to the

top of the heat exchanger. A program to solve the equations was written using MATLAB SIMULINK. The program returns the distribution of all calculated parameters for the respective element numbers.

Some assumptions are made when deriving this model. The following is a list of assumptions:

1. Air is an ideal gas; this is a reasonable assumption, since the heat exchanger is open to the atmosphere and the air pressure is assumed to be constant throughout it. The ideal gas properties were used in all equations for air in the model.
2. No heat is lost from the heat exchanger to the surroundings. This assumption is made to simplify the model and reduce the number of equations. It was assumed that the heat exchanger is well insulated; therefore it would result in minimal heat losses. This assumption is reasonable since the heat exchanger's surface area is relatively small, due to its small dimensions. This will be shown in the next chapter, and therefore it will result in a negligible amount of losses.
3. Radiation heat transfer is neglected; this assumption can be justified by assuming that the inner wall of the heat exchanger does not absorb any thermal radiation. The radiation heat losses from both ends of the heat exchanger can also be neglected, since the ratio of the heat exchanger's height to diameter is high. Thus, a minimum amount of radiation will escape. Finally, the droplets are scattered in the heat exchanger volume, and there is a relatively large distance between them with respect to their diameter. Therefore, the resulting view factors would be low.

4. No breakup of the droplets occurs and the droplets maintain a spherical shape. This assumption is reasonable since the ratio of the droplet's viscosity to the air viscosity is very high, over 140, which will assure no breakup or shape distortion of the droplet. Also, the Reynolds number in the heat exchanger does not exceed 300, which is much less than 1,000, the value where liquid metal droplets start to distort and eventually break up.
5. No mass transfer occurs from the droplets to the air. This assumption is reasonable since the vapor pressure of CuCl is very low. It has a value of 10 Pa at a temperature of 459 °C, and increases to 100 Pa at 543 °C. So the average vapor pressure value, over the temperature range where the droplet is in liquid phase, is low. Therefore, mass transfer from the droplet can be neglected.
6. The droplets have a uniform temperature. This means that no temperature gradients exist within the droplets. This is assured by maintaining Bi less than 0.1. This will be shown in the model constraints section.

### 3.5.1 Solution Procedure

Figure 3.6 shows a diagram of the solution procedure throughout the heat exchanger. This procedure was repeated for every element until the CuCl temperature reached its maximum value. Then the final inlet droplet velocity is compared to the actual inlet droplet velocity, based on the mass flow rate of CuCl. If the velocities are the same, then the temperature distribution, velocity distribution, and all other calculated parameters have properly converged. Otherwise, a new iteration of the exit droplet temperature is tried, and the program is repeated again until a match in the droplet inlet velocity is reached. The height of the heat exchanger is found at the end

by multiplying the number of elements to reach the maximum CuCl temperature and the element height.

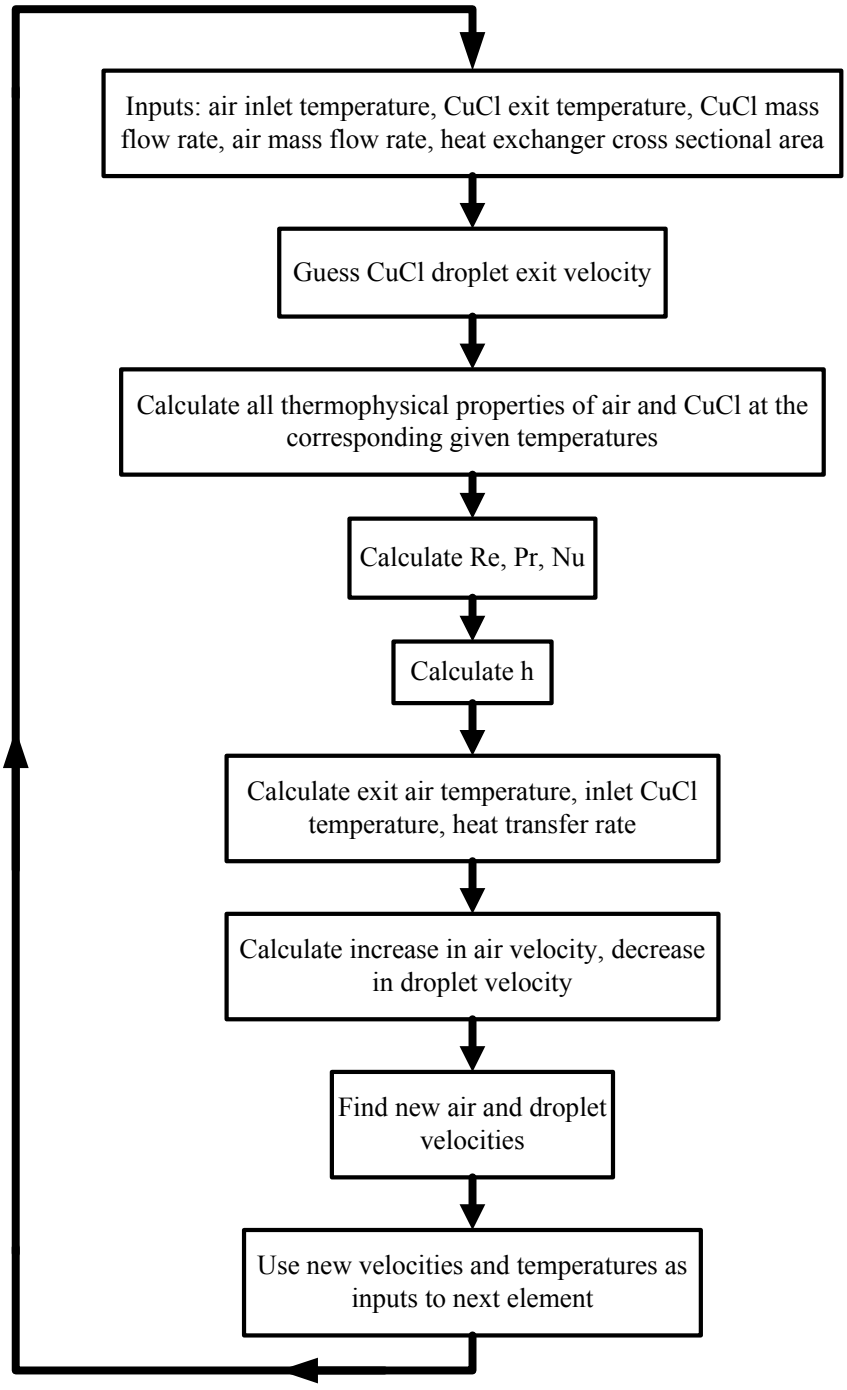


Figure 3.6 Model solving procedure diagram for the heat exchanger.

### 3.5.2 Model Constraints

In order to assure that the assumptions remain valid throughout the heat exchanger, there are a number of constraints that are enforced in the program. The model is solved within the limits of these constraints. The following is a list of model constraints:

1. Minimum air mass flow rate: the air mass flow rate was limited to not be smaller than the minimum value required to recover all heat from the CuCl. The values of the minimum flow rate were determined by applying the first law of thermodynamics to the heat exchanger. The CuCl inlet and exit temperatures were set constant to 530 and 70°C, respectively. The air inlet temperature was varied from 25 to 70°C, and the air flow rate to recover all energy from the CuCl was found. Figure 3.7 shows a plot of the minimum air flow rate, per kilogram of CuCl, versus the air inlet temperature,
2. Maximum temperature difference across each element: as explained in the previous section, all properties of the fluid and CuCl are evaluated at the inlet air temperature and exit CuCl temperature, respectively, in each element. Then these properties were used to find the unknown temperatures and velocities. If the temperatures of both substances were allowed to have large changes in their values across each element, a non-continuous trend in the properties was observed. This leads to errors in the calculations. Therefore, the flow configurations had a minimal temperature change across each element, while satisfying the other constraints of the model. The temperature changes of the fluid and CuCl across each element were kept to a maximum of a 3 °C change, to eliminate the above discussed errors.

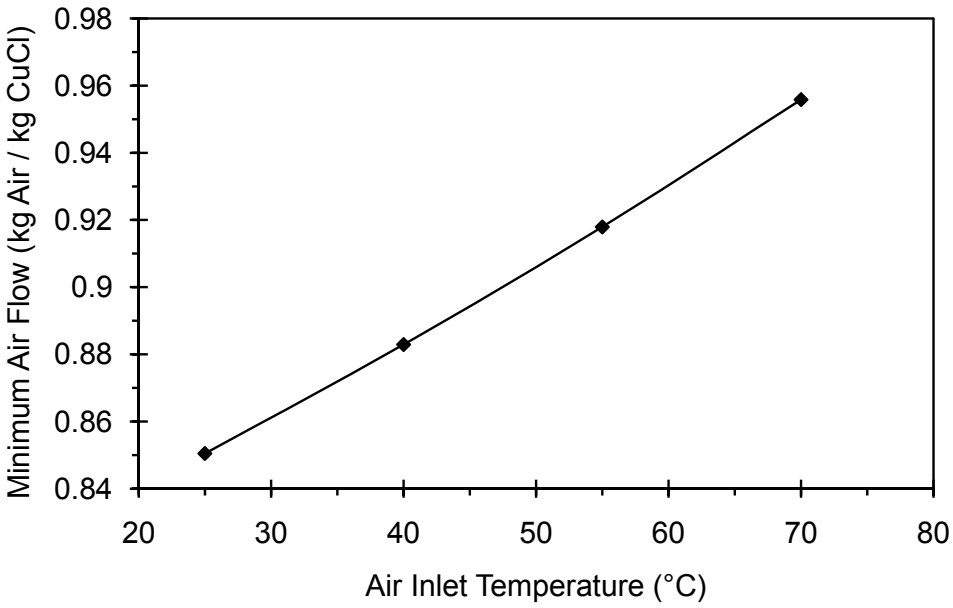


Figure 3.7 Minimum air flow rate versus air inlet temperature.

3. Lumped capacitance: as explained earlier, the model assumes lumped capacitance for the CuCl droplets. For this to be valid, the Biot number for the droplets was kept less than 0.1 throughout the heat exchanger in all simulations, by changing the heat exchanger's dimensions. Two parameters can be controlled to reduce the Biot number: the droplet diameter and the convection heat transfer coefficient. A smaller droplet diameter and convection heat transfer coefficient leads to a lower Biots number. Figure 3.8 shows the maximum convection coefficient for a set of droplet diameters versus the CuCl droplet temperature. For a lower droplet size, a higher convection heat transfer coefficient arises. A higher convection heat transfer coefficient means that higher flow and droplet velocities can be achieved.

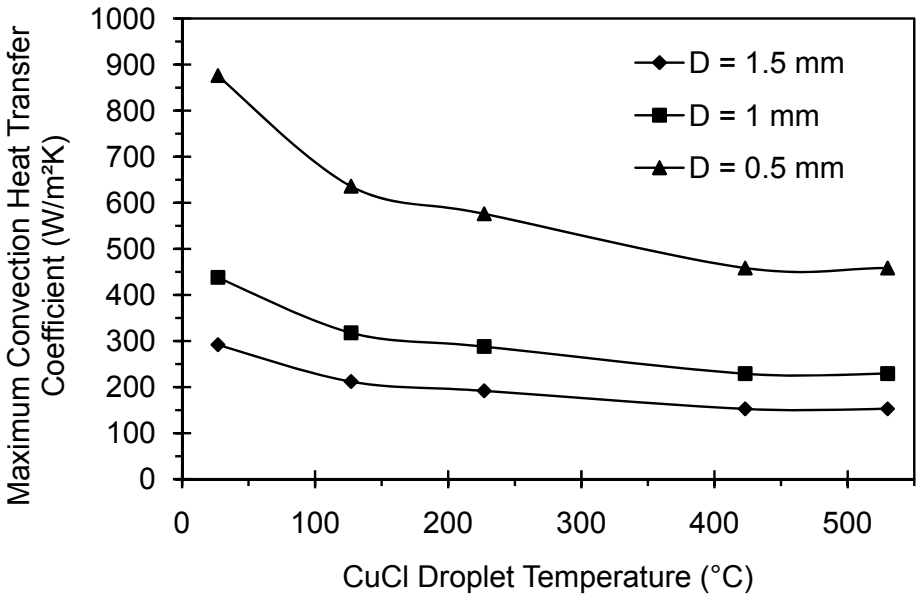


Figure 3.8 Maximum convection heat transfer coefficient versus droplet temperature.

### 3.5.3 Other Functions

Apart from the equations shown in the model formulation, the only other functions and equations used in the model are those to calculate the different properties of CuCl and air. The following is a list:

1. CuCl Properties: the CuCl parameters are the specific heat, specific enthalpy, thermal conductivity, density and the CuCl droplet diameter. All of these parameters are functions of temperature. Various studies on the different CuCl thermal properties can be found in [62-64]. Figures 3.9 to 3.13 show how the specific heat, specific enthalpy, thermal conductivity, density, and droplet diameter of CuCl vary with temperature, respectively. A best fit was generated for each of these graphs using polynomial functions. In the case where a best fit with high accuracy could not be found for the entire temperature range, as in the case where the properties change drastically after the phase change processes, then the temperature range would be broken up and multiple

polynomials were used to fit the data. The polynomials were used in the model as the property functions.

2. Air properties: the air properties of importance for the analysis are density, specific heat, specific enthalpy, specific volume, thermal conductivity, and viscosity. All of these properties are a function of temperature. The ideal gas air properties were taken from EES software. Then a best fit for each of the properties was found using a polynomial function. The polynomials were then used in the model as the air property functions, like the CuCl property functions. A comparison is made between ideal and real air properties in appendix A, the comparison shows good agreement between real and ideal air properties, thus, the use of ideal air properties is justified.

Figure 3.9 shows how the specific heat of CuCl varies with temperature. Because CuCl exists in three phases, two solid phases and one liquid phase, there are three different curves for the specific heat representing each phase. Up to a temperature of 412°C, CuCl exists in a solid c phase. At 412°C, it changes phase to solid β phase. In this phase, CuCl remains solid, but with a different microstructure that has different thermophysical properties. Solid β phase exists in the temperature range of 412 - 423°C. At 423°C, it changes phase again to liquid phase, and it remains in a liquid phase up to the maximum temperature in the Cu-Cl cycle, 530°C. The specific heat for the solid phases increases with increasing temperature, with the solid β phase having a higher specific heat than the solid c phase, while the specific heat of the liquid phase decreases with increasing temperatures. Figure 3.10 shows how the specific enthalpy of CuCl varies with temperature. The enthalpy increases linearly with temperature up to a temperature of 412°C, where it changes phase. The sudden

change in the enthalpy value at this temperature is equal to the latent heat of this phase change process. Then, the enthalpy increases linearly with temperature up to 423°C, where CuCl changes phase to liquid. Again, the sudden change in enthalpy is equal to the latent heat of the phase change process. The value of the specific enthalpy keeps increasing linearly with temperature. Figure 3.11 shows the variation of the thermal conductivity of CuCl with temperature. The thermal conductivity decreases with increasing temperature nonlinearly in the solid phases. In the liquid phase, the thermal conductivity has a nearly constant value. Figure 3.12 shows the density variation with temperature for CuCl. The density of the solid phases decreases with increasing temperature, while it is almost constant for the liquid phase, because the rate of density decrease with temperature for the liquid phase is very small, therefore the density change is neglected. Also, Figure 3.13 shows the variation of the droplet diameter with temperature for the two droplet diameter cases studied, 1 and 0.5 mm.

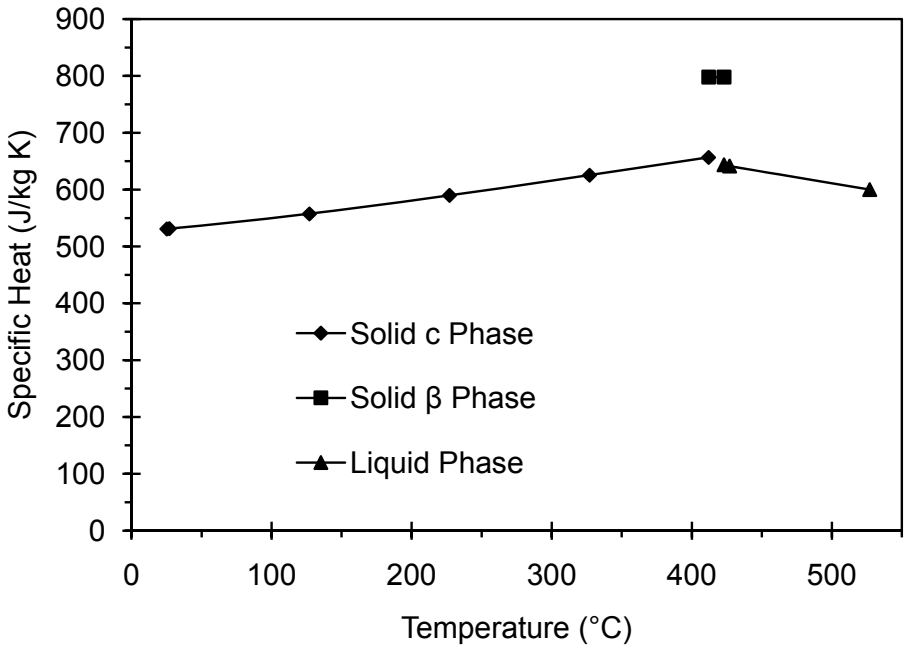


Figure 3.9 CuCl specific heat variation with temperature.

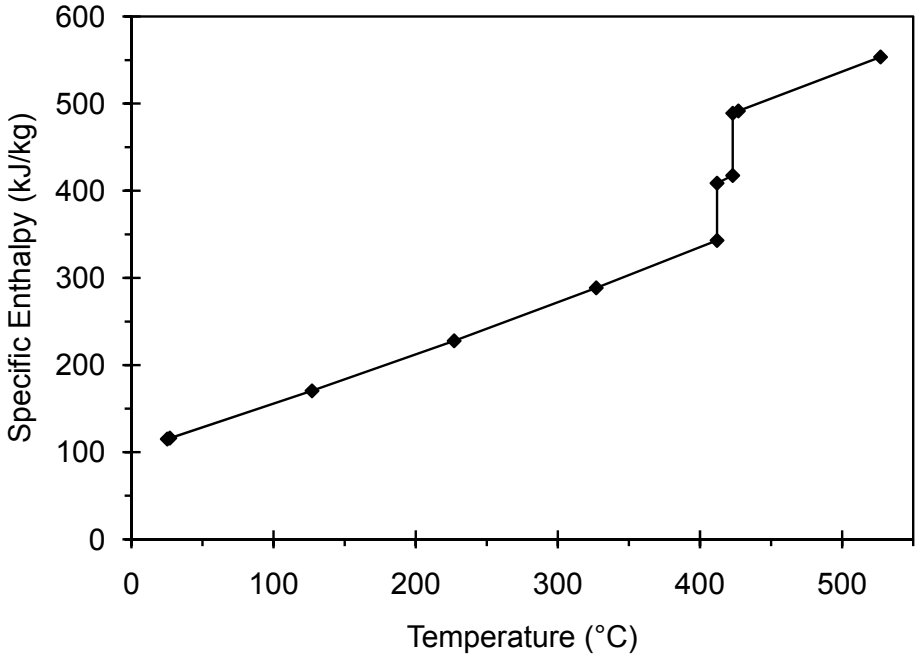


Figure 3.10 CuCl specific enthalpy variation with temperature.

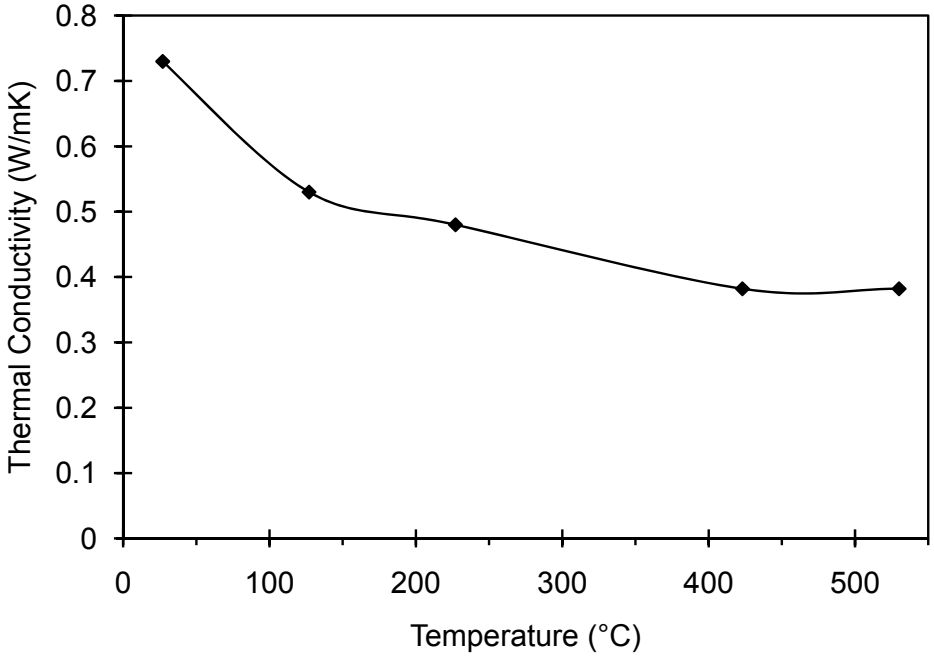


Figure 3.11 CuCl thermal conductivity variation with temperature.

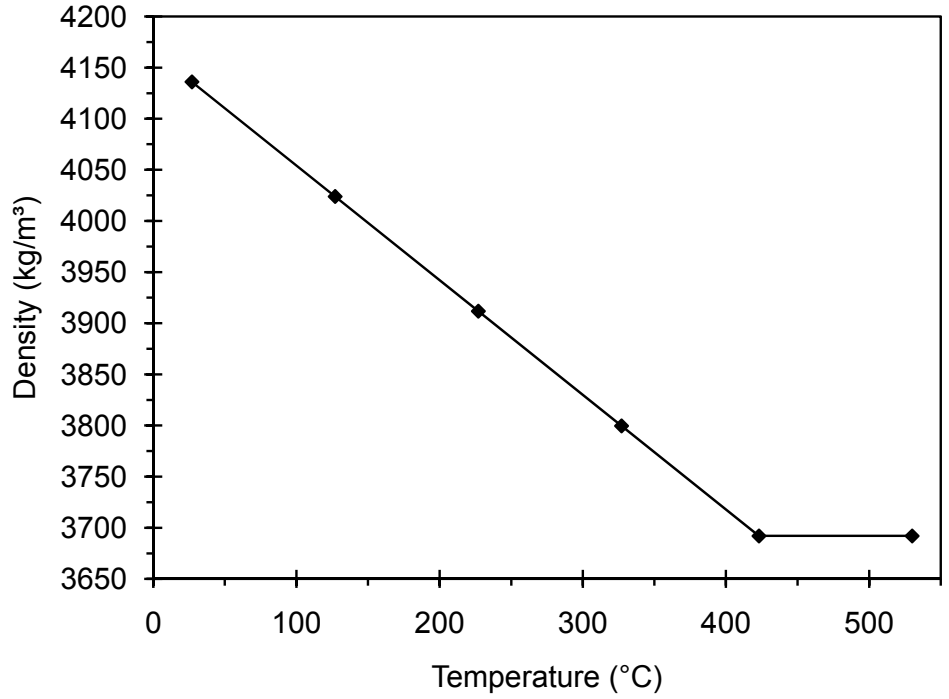


Figure 3.12 CuCl density variation with temperature.

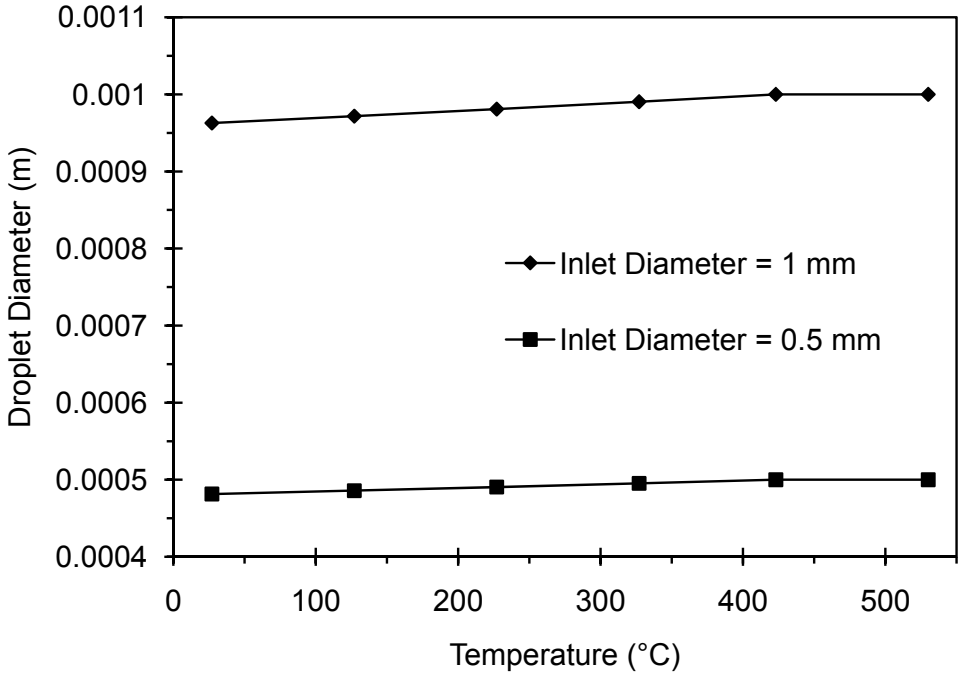


Figure 3.13 CuCl droplet diameter variation with temperature.

All of the property polynomials had a coefficient of determination ($R^2$) greater than 0.99 to assure high accuracy.

## 3.6 Summary

The simulation process is a long iterative process. The program had to be run several times before obtaining a steady solution, in order that the heat transfer, fluid and droplet flow problems stay within the model restrictions. Because of the two phase change processes that a droplet passes through, two programs were used to analyze the heat transfer process: one for sensible heat transfer, and the other for latent heat transfer. The sensible heat transfer program was run first, from the bottom of the heat exchanger to the point where the CuCl temperature reaches its second phase transformation temperature. Then the final outputs of the program were taken as inputs to the latent heat transfer program, which was then run until the air temperature reached a value that satisfies the first law of thermodynamics. This requires the change in total energy of air between the input and output to be equal to the amount of latent heat released by the CuCl. The outputs from this were taken back to the sensible heat program as inputs, which was then run again until the CuCl temperature reached its first phase transformation temperature. The final results were taken back to the latent heat transfer program as inputs again, and it was run until the air temperature reached a value that satisfies the first law of thermodynamics. Then the outputs were finally taken to the sensible heat transfer program as inputs. This was run until the CuCl temperature reached the inlet temperature to the heat exchanger of 530°C. This process was repeated for every trial of inputs to the heat exchanger; inlet air and exit CuCl temperatures, inlet air and droplet exit velocities, air and CuCl mass

flow rates, and droplet diameter throughout the heat exchanger. This was a long iterative process, with tight restrictions on parameters.

In the next chapter, two cases of droplet diameters (1 and 0.5 mm) will be studied. The temperature, velocity, Re, Nu, convection heat transfer coefficient, droplet acceleration, drag coefficient and force, and the heat transfer rate and flux variations throughout the heat exchanger height will be found. The dimensions of the heat exchanger will also be found.

# Chapter 4

## Results and Discussion

### 4.1 Model Validation

The results of the simulations could not be directly validated for molten CuCl, due to the lack of similar data on heat exchangers of the same type in past literature. No measured data was available either for molten CuCl, so no experimental results were available for comparison with the simulated theoretical results. However, the trends of the temperatures in the sensible heat transfer regions throughout the height of the heat exchanger follow the same trends as those presented in [61].

To validate the program, a problem presented in [65] to find the heat transfer rate from a droplet in an air flow was solved. Table 4.1 shows the results presented in [65] and data obtained using the convenient program. The relative error between both results is also shown. The heat transfer rate in the final row was not calculated in [65]. However, the calculated convection heat transfer coefficient was used to find the instantaneous heat transfer rate to compare with the calculated heat transfer rate provided by the program.

From the table, both results agree well. The maximum relative error is 1.7%, for the heat transfer rate. The errors are well within practical limitations, which provides useful validation of the new model. The main source of errors is the accumulated error when numbers are rounded up during calculations. When higher accuracy in the calculations is needed, by taking more significant digits after the decimal point, a lower relative error will be obtained.

Table 4.1 Program result validation.

| Parameter | Reference [65] | Program simulation result | Relative error |
|---|---|---|---|
| **Re** | 6440 | 6457 | 0.3 % |
| **Nu** | 47.1 | 47.3 | 0.4 % |
| **Convection heat transfer coefficient ($W/m^2K$)** | 118 | 120 | 1.7 % |
| **Heat transfer rate (W)** | 1.9 | 2 | 1.7 % |

## 4.2 Fluid and Droplet Flow Results

Fluid and droplet flow affects the heat transfer process significantly. Heat transfer is a result of the fluid and droplet motions. The results of interest for the fluid and droplet flows are the velocity profiles and the acting forces on the droplet, throughout the height of the heat exchanger. The problem parameters are summarized in Table 4.2 at the end of the chapter.

Figure 4.1 shows the velocity profile of a droplet, with a diameter of 1 mm, in the heat exchanger, along with the air velocity profile. The figure shows the droplet velocity, air velocity components, air inlet velocity, air expansion velocity, and the relative velocity. The droplet enters the heat exchanger with a small velocity, about 0.02 m/s, which is the CuCl flow velocity at the top of the heat exchanger. After this point, two forces act on the droplet, which are the weight of the droplet and the drag force from the air flow. The droplet accelerates as it moves downwards to reach a final exit velocity of about 3.2 m/s. The acceleration of the droplet throughout the

height of the heat exchanger is not constant. It varies greatly, based on the difference between the downward gravitational acceleration and the upward acceleration, caused by the drag force. At the top of the heat exchanger, the downward acceleration is maximum, because the relative velocity is lowest at the top. The drag force and its resulting upward acceleration are lowest there. This causes the droplet to reach high velocities in a very short time, as noticed from the high rate of increase of the droplet's velocity at the top of the heat exchanger. The rate of the droplet's velocity increase falls with distance traveled, due to the increase of the drag force and its resulting upward acceleration, which decreases the net downward acceleration. However, the rate of the droplet's velocity increase is always positive, meaning that the droplet is always accelerating downwards.

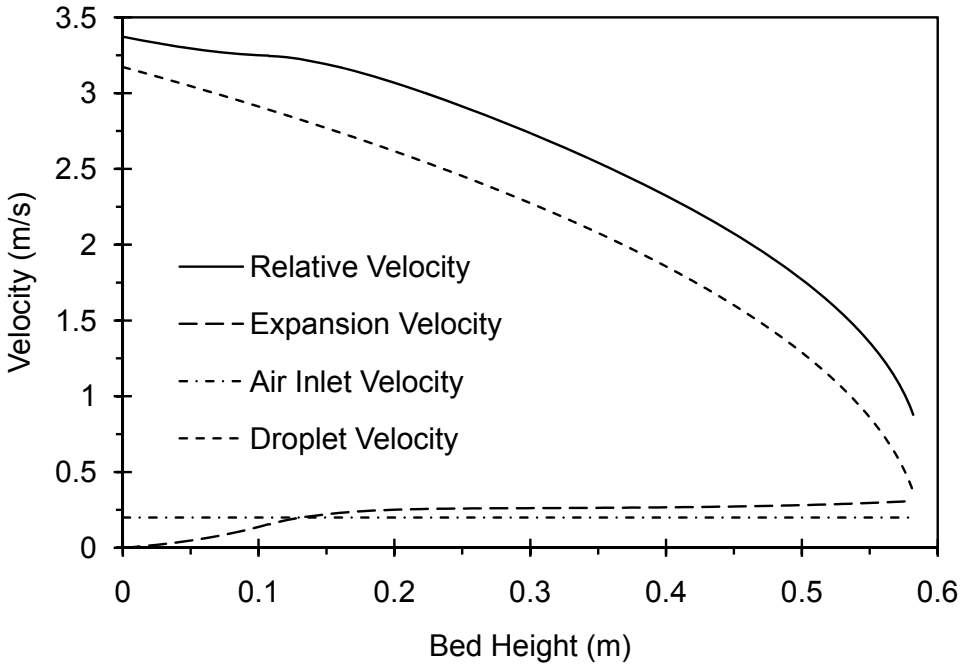


Figure 4.1 Velocity profiles for a droplet with a 1 mm diameter.

The air inlet velocity is constant throughout the height of the heat exchanger, with a value of 0.2 m/s. This air velocity component is not affected by the temperature changes of the air stream, as explained in the previous chapter. The air expansion velocity is 0 m/s at the bottom of the heat exchanger, and increases to 0.31 m/s at the top of the heat exchanger. The variation of this component of the air velocity is due to the temperature change of air along the height of the heat exchanger. This causes the air to expand, and since the air can only expand in the upward direction, its velocity increases. The air expansion velocity increases at a high rate at the bottom part of the heat exchanger. This is due to the high temperature changes of air, which are driven by the high heat transfer rate at this part, which causes a high rate of expansion. The rate of velocity increase falls along the height, which is due to the lower air temperature variations. It almost reaches a constant value of 0.26 m/s in the CuCl's first phase transformation section of the heat exchanger. Then the rate of increase starts rising again at the end of the heat exchanger, due to the high air temperature changes in that region.

Finally, the relative velocity, which represents the sum of all velocities, varies largely with height. Moving up from the bottom of the heat exchanger, the relative velocity initially decreases at a high rate. The decrease rate slows down, due to the higher rate of increase in the expansion velocity than the decrease rate in the droplet's velocity, until it reaches a value of zero. Then, the rate of decrease in the relative velocity starts increasing again, because the air temperature variations reach values that cause the rate of increase in the expansion velocity to be lower than the rate of decrease in the droplet's velocity. The relative velocity keeps on decreasing at an increasing rate after this point up to the top of the heat exchanger, were it reaches a value almost equal to the air velocity of 0.51 m/s.

Figure 4.2 shows the velocity profile of a 0.5 mm droplet, along with the air velocity and total velocity. The trends of the changes of each of the velocities is the same as for a droplet with a diameter of 1 mm. The same discussion applies to this case too. The droplet however, in the case of a 0.5 mm diameter, reaches higher velocities at the bottom of the heat exchanger, because the heat exchanger height for the smaller diameter droplet case is larger. This means the droplet stays in the heat exchanger for a longer time, and therefore will reach higher velocities. Another reason is the lower drag force that a smaller droplet experiences, mainly because of the much smaller cross-sectional area. This causes the upward acceleration to be lower and the net downwards acceleration higher, which will cause the droplet to reach higher velocities.

In this case, the droplet inlet velocity was higher than the previous case with a value of 0.07 m/s, and an exit velocity at the bottom of the heat exchanger of 3.7 m/s. The air expansion velocity reaches the same value as the previous case at the top of the heat exchanger, 0.51 m/s. The air inlet velocity for this case was the same as the previous case, 0.2 m/s. Finally, the relative velocity is much higher for a smaller diameter droplet, because of the larger droplet velocities. The relative velocity had a value of 3.9 m/s at the bottom of the heat exchanger, and a value of 0.58 m/s at the top of the heat exchanger.

Figure 4.3 shows the drag coefficient variation throughout the heat exchanger's height, for droplets with a 1 and 0.5 mm diameter. It can be noticed that a droplet with a smaller diameter has a higher drag coefficient. This is because a droplet with a smaller diameter generally has a lower Reynolds number, even though the relative velocity for a smaller diameter droplet is generally higher. On the standard drag coefficient curve, the drag coefficient for a smaller droplet diameter will always

stay at the left side, meaning it will be in the region where the drag coefficient is higher.

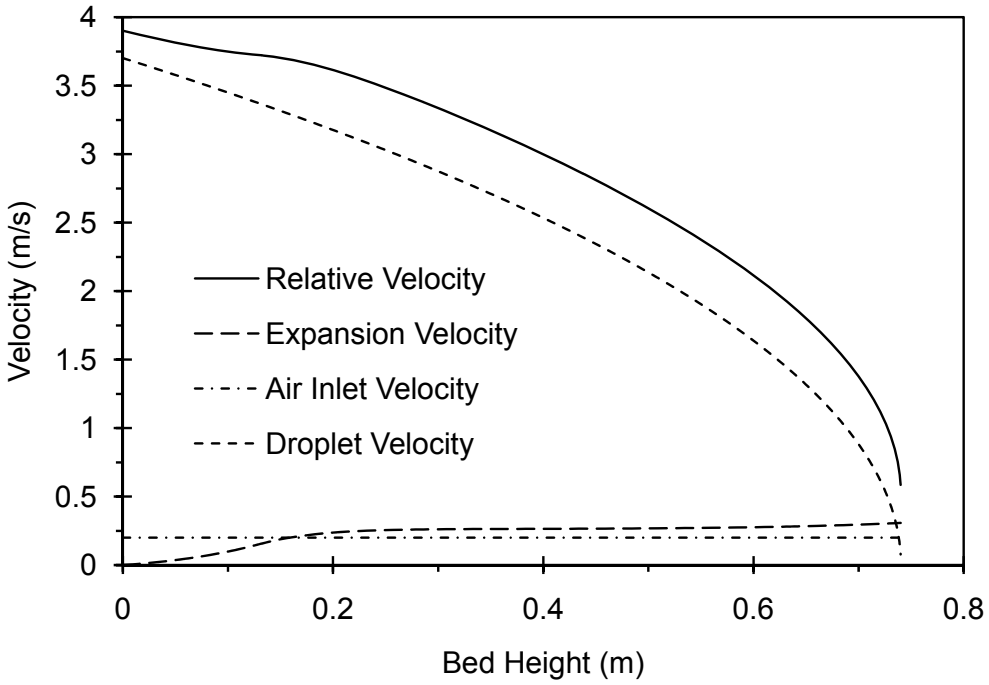


Figure 4.2 Velocity profiles for a droplet with a 0.5 mm diameter.

The difference between the drag coefficients of both droplets is almost constant up to the region in the heat exchanger where the droplet velocity increase rate is high, in the top region of the heat exchanger. In this region, the drag coefficient for a smaller diameter droplet increases at a much higher rate, which is due to the much higher rate of change of the relative velocity caused by the high rate of change of the droplet's velocity. The drag curves follow the general trend of the standard drag curve. At the bottom of the heat exchanger, the Reynolds number is at its maximum, due to the high total velocity. This generates a drag coefficient that is low. Moving upwards in the heat exchanger, the Reynolds number decreases, due to the decrease in

the relative velocity, which causes the drag coefficient to increase. The change in the increase rate of the drag coefficient is caused by the change in the decrease rate of the relative velocity throughout the heat exchanger. For a droplet with a smaller diameter, this does not mean it will experience a higher drag force, even though it has a slightly higher drag coefficient, as shown in Figure 4.4. The figure shows the drag force variation for a droplet with 1 and 0.5 mm diameter throughout the height of the heat exchanger.

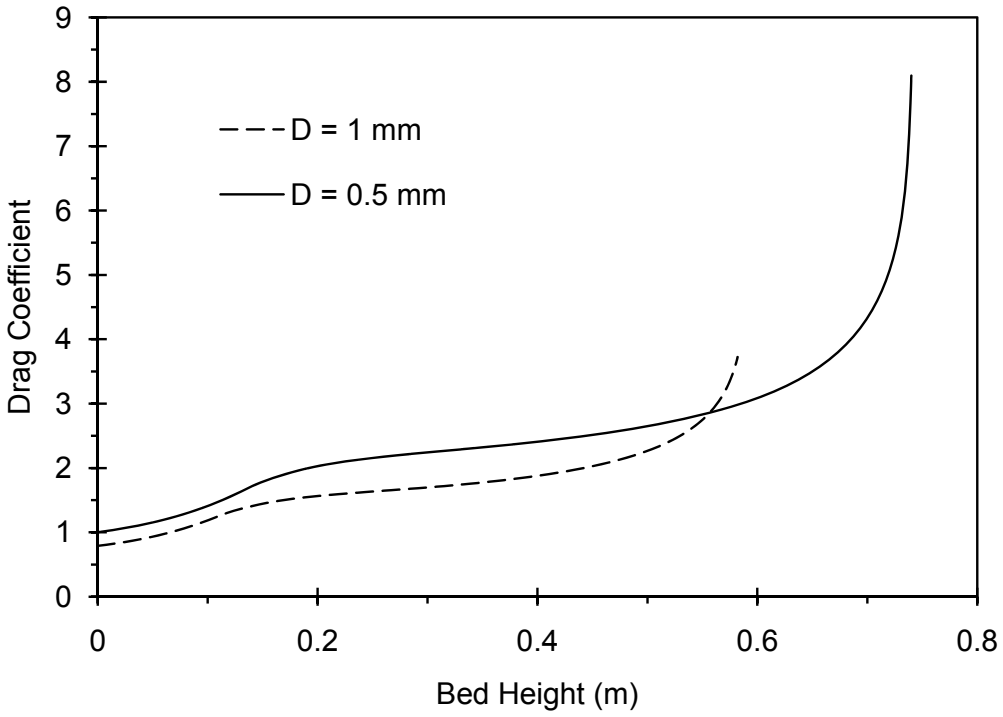


Figure 4.3 Drag coefficient variation with bed height.

It can be observed that droplets with a larger diameter undergo a larger drag force, even though their drag coefficient is slightly lower. The main reason is the much larger cross sectional area of larger diameter droplets. When comparing droplets with a diameter of 1 and 0.5 mm, the droplet with a 1 mm diameter has four times the

area of a droplet with 0.5 mm diameter. Thus, under the same flow conditions, the drag force on a 1 mm droplet will be generally four times higher than the drag force on a 0.5 mm droplet diameter.

From Figure 4.4, the drag force is decreasing along the height of the heat exchanger at different rates. At the bottom of the heat exchanger, the rate of change of the drag force is decreasing. This can be explained by the drag force equation, equation (3.6). This assumes that the fluid density variation for both droplets, with diameters of 1 and 0.5 mm, is constant. The drag force will be determined by the combination of effects of the area, drag coefficient, and relative velocity. Because of the large effects of the temperature variation on the expansion velocity, and therefore the relative velocity, and since the velocity values in this region are high, the rate of decrease of the relative velocity will cause the drag force to decrease with a high rate. Since the rate of decrease in the relative velocity decreases as air temperature variations become lower, the drag force decreases at a lower rate. After this region, the drag force decreases at an increasing rate, due to the rate at which the relative velocity is decreasing.

The drag force curve for the 1 mm diameter droplet crosses that drag force curve for the 0.5 mm droplet. This occurs at the point where the relative velocity reaches very low values for the 1 mm droplet. The 0.5 mm droplet still has large values of velocity, so the effect of the larger cross-sectional area diminishes. Also, the increasing drag coefficient values for the smaller droplet begin to have large effects on the drag force for the 0.5 mm droplet. The overall effect leads to reduce the drag force for the 1 mm droplet at a rate that is higher than that of the 0.5 mm droplet. The drag force might seem negligible because of the small values. However, this force generates a high upward acceleration that cannot be neglected.

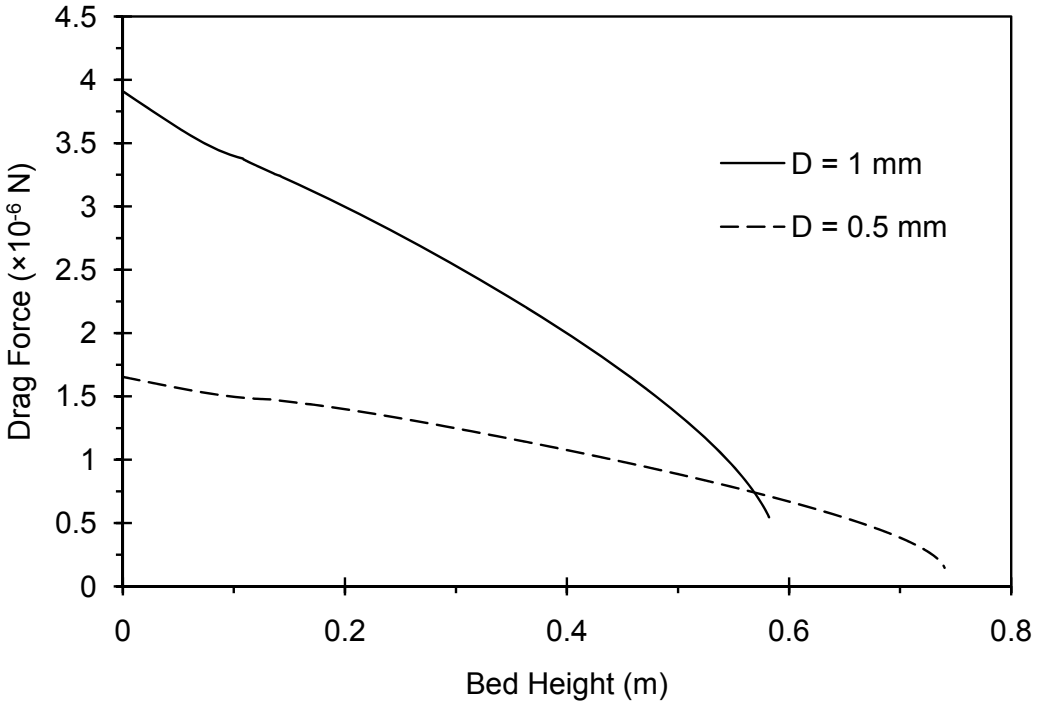


Figure 4.4 Drag force variation on each droplet.

Figure 4.5 shows the variation of the droplet's acceleration throughout the height of the heat exchanger, for a droplet with a diameter of 1 mm. The downward acceleration, which is the resultant droplet acceleration, is equal to the difference between the gravitational acceleration and the upward acceleration caused by the drag force on the droplet. Since the droplet enters the heat exchanger with a very low velocity, the upward acceleration caused by the drag force is low. Thus, the downward acceleration of the droplet is very close to the gravitational acceleration. As the droplet builds up velocity, the upward acceleration increases, which leads to a decrease in the downward acceleration of the droplet. The maximum droplet downward acceleration is 9.5 $m/s^2$, which occurs at the bottom of the heat exchanger. The upward acceleration, which can be obtained by dividing the drag force by the droplet mass, has a maximum value of 2 $m/s^2$. This occurs at the bottom of the heat

exchanger, and a minimum value of 0.3 $m/s^2$, This occurs at the top of the heat exchanger. The rate at which the upward acceleration decreases is proportional to the rate at which the relative velocity decreases at. It has a low rate of change initially, but the rate of decrease rises towards the top.

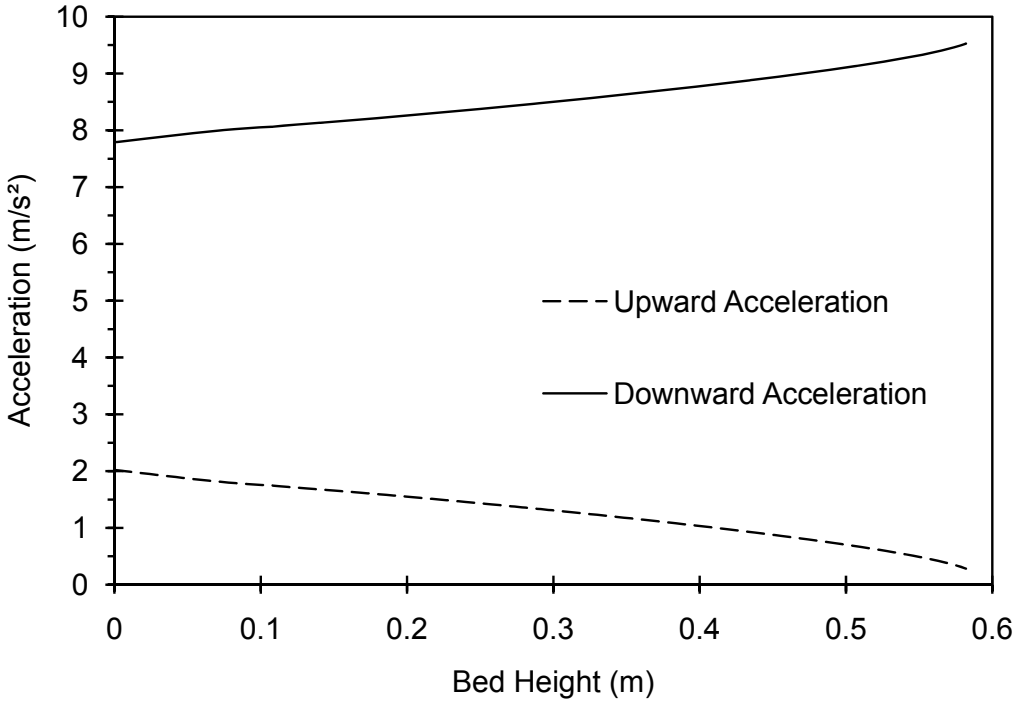


Figure 4.5 Acceleration of a droplet with a 1 mm diameter.

Figure 4.6 shows the variation of the upward and downward accelerations for a droplet with a diameter equal to 0.5 mm. The trend of the change (both upward and downward accelerations) is the same as that of a droplet with a diameter of 1 mm. However, the values of the downward droplet acceleration are generally larger than that of a droplet with a 1 mm diameter. Again, the droplet has an acceleration close to the gravitational acceleration at the top of the heat exchanger. It decreases as the droplet moves downwards, and reaches a final value at the heat exchanger's bottom of

8.95 m/s$^2$. The upward acceleration caused by the drag force has a minimum value of 0.05 m/s$^2$ at the top of the heat exchanger, and a maximum value of 0.86 m/s$^2$ at the bottom of the heat exchanger. The lower upward acceleration for a droplet with a smaller diameter is due to the lower drag force. The higher downward acceleration of a droplet with a smaller diameter is the reason for it obtaining higher velocities and higher relative velocities. A final note on the differences between the accelerations of droplets with different diameters is the rate at which the difference between the downward and upward accelerations changes. The upward and downward accelerations of droplets with larger diameters converge much faster than that of small diameter droplets.

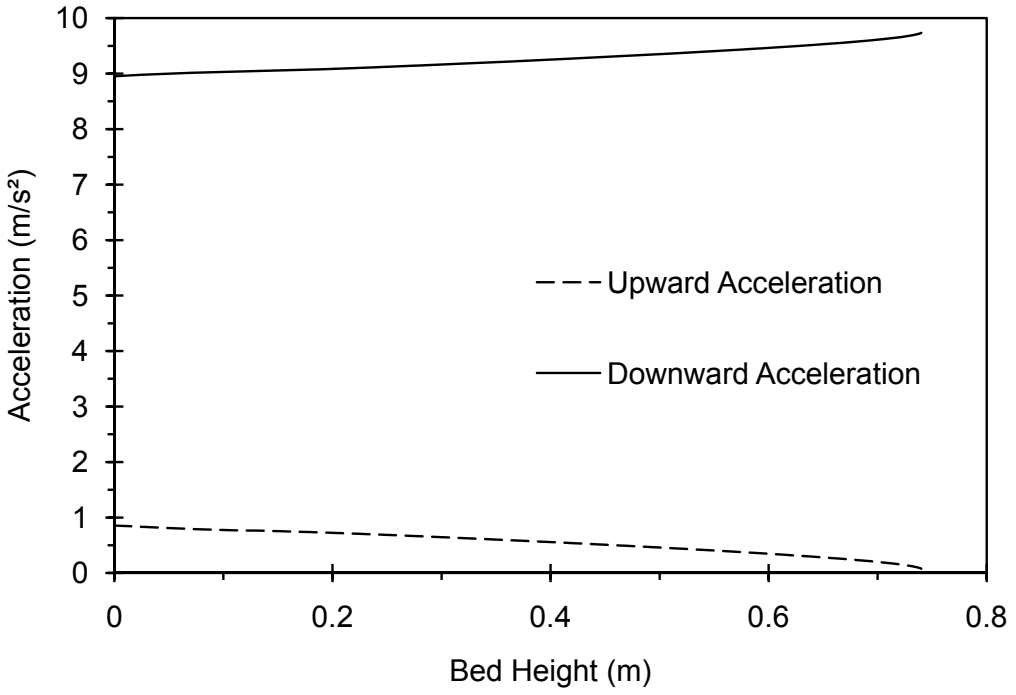


Figure 4.6 Acceleration of a droplet with a 0.5 mm diameter.

## 4.3 Heat Transfer Results

After knowing the flow characteristics of the fluid, air, and droplets, the heat transfer problem can be solved. A goal of analyzing the fluid and droplet motions is to find the Nusselt number, which would determine the convection heat transfer coefficient, and then the temperature distribution can be determined.

Figure 4.7 shows the temperature distribution for air and the CuCl droplet stream, for a droplet diameter of 1 mm, throughout the heat exchanger height. The figure shows five heat transfer processes, moving up from the bottom of the heat exchanger. These are sensible heat transfer from the CuCl droplets to the air stream, latent heat transfer from the droplets to the air stream at a CuCl droplet stream temperature of 412°C, then another sensible heat transfer process from the droplets to the air stream, followed by another latent heat transfer process at a CuCl droplet temperature of 423°C. Finally, there is a sensible heat transfer process again from the CuCl droplets to the air stream.

In the first sensible heat transfer process, heat is transferred from the CuCl droplets to the air stream. In this process, the air and CuCl droplet temperature increases with height. The rate at which they increase is also increasing, with the CuCl droplet temperature increasing almost twice as fast as the air temperature. This occurs because the CuCl specific heat is roughly half that of air, so for a one degree change in air temperature to occur across one element, the CuCl droplet temperature has to increase by two degrees. This is required to satisfy the first law of thermodynamics, and explain why that the temperature difference between both streams increases with increasing height.

Figure 4.7 was generated for a CuCl flow of 3.4 g/s, which is equivalent to the flow from an oxygen production reactor for a hydrogen plant generating 3 kg of

hydrogen per day. The air flow rate is 3 g/s, which is slightly higher than the minimum air flow required to recover all heat from a stream of CuCl droplets at a temperature of 530°C. Because of the high average temperature difference between the CuCl droplets and air streams, the heat transfer rate is high. Once the CuCl droplet stream reaches a temperature of 412°C, the second phase transformation process occurs. Here CuCl droplets change phase from solid c phase to solid β phase. In this process, the CuCl droplet temperature is held constant at the phase transformation temperature. The air temperature increases, but with a decreasing rate of increase, because when the air temperature increases, the temperature difference between both streams decreases and causes the heat transfer rate to decrease. This causes the required length of interaction between both streams to recover one unit of thermal energy to increase.

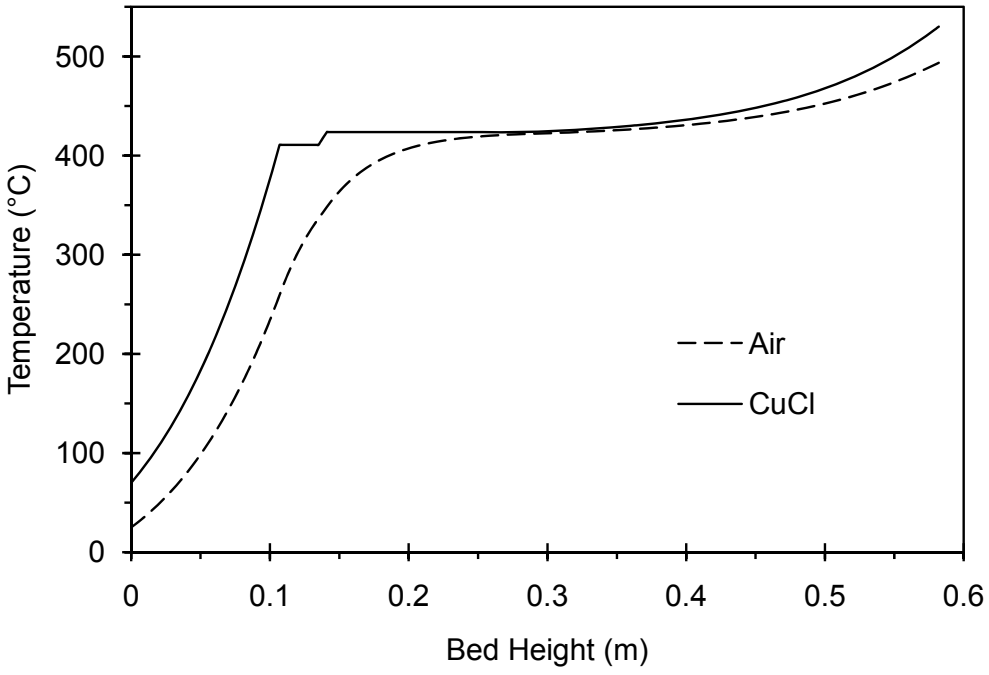


Figure 4.7 Temperature distribution for CuCl droplets with 1 mm diameter.

The heat transferred to the air stream from the droplet stream in the first sensible heat transfer process is more than three times the amount of heat transferred in this latent heat transfer process. This implies that the average required length to transfer one unit of thermal sensible energy was about 0.02 m, compared to 0.03 m to transfer the same amount of heat in a latent heat transfer process, with the same inlet temperature difference. When all of the latent energy released by the CuCl droplets is absorbed by the air stream, a new sensible heat transfer process occurs. Here, sensible heat is transferred from the droplets to the air stream. The temperature difference between both streams starts to increase again, for the same reason stated earlier, and the heat transfer rate increases. The CuCl droplet temperature does not increase much, because the first phase change transformation process occurs at a temperature of 423°C, so the CuCl droplet temperature only changes by about 11 degrees. In this phase transformation process, CuCl droplets change phase from liquid phase to solid β phase. This process occurs at a constant CuCl droplet temperature of 423°C. In this process, the air temperature increases at a slow rate, because of the decreasing rate in temperature difference between both streams, which causes the heat transfer rate to decrease. The rate at which the air temperature increases keeps decreasing until it almost reaches a value of zero. This happens at the end of the process, where the air temperature reaches a value of 422°C. This point has the lowest heat transfer rate throughout the heat exchanger.

The final sensible heat transfer process starts when all latent heat energy is absorbed by the air stream from the first phase change process. In this final process, the CuCl droplets and air temperatures start increasing with an increasing rate, similar to the temperature increase in the first sensible heat transfer process. The temperature difference between both streams also increases. The process ends when the CuCl

droplets reach a temperature equal to 530°C and the air reaches a temperature of about 493°C. The required dimensions for the heat exchanger to complete all of the heat transfer processes are a height of 0.6 m and a diameter of 0.13 m.

Figure 4.8 shows the temperature distribution for the air and CuCl droplet stream for droplet diameters of 0.5 mm. The temperature variations throughout the heat exchanger follow the same trend as the previous figure. The difference between both graphs is that the required interaction length between the CuCl droplets and air is slightly larger for the case of 0.5 mm droplet diameters, than for the case of droplets with 1 mm diameters. This occurs because the heat transfer rate from droplets with a 0.5 mm diameter is less than that of droplets with a 1 mm diameter. The reason behind is that a droplet with a diameter of 1 mm has eight times the surface area of a droplet with a 0.5 mm diameter. The same discussion for the temperature variations of both streams applies for the case of droplets with a 0.5 mm diameter, as that of droplets with a 1 mm diameter. The CuCl and air mass flow rates are the same as the previous case. The required dimensions of the heat exchanger for the case of a 0.5 mm droplet diameter are a height of 0.8 m and a diameter of 0.13 m.

Figure 4.9 shows the variation of Reynolds number throughout the height of the heat exchanger for droplets with 1 and 0.5 mm diameters. The variation of Reynolds number involves the variations of the droplet diameter, relative velocity and the kinematic viscosity of air. From the graph, one can see that Re decreases throughout the height. The rate of decrease is initially high at the bottom of the heat exchanger. It decreases with increasing height until the top region of the heat exchanger is reached, and then the rate of decrease starts increasing again until the lowest Reynolds number is reached at the heat exchanger top. This variation can be explained as follows. In the entrance region of the heat exchanger, where the first

sensible heat exchange takes place, the relative velocity is high. It decreases, but at a slow rate. The air temperature increases at a high rate, which causes the kinematic viscosity to increase at a high rate too. Therefore, the combination of the slowly decreasing velocity and the rapidly increasing viscosity lead to the high rate in decrease of Re. Moving up the heat exchanger, the relative velocity starts decreasing at a higher rate, and the air temperature increases, but at a slower and slower rate, which causes the rate of increase in the air viscosity to slow down and reach a value near zero. This makes the rate of decrease of Reynolds number lower and lower. At the top of the heat exchanger, the relative velocity decreases rapidly and the air temperature increases at a high rate, making the air viscosity increase at an equally high rate, making the Reynolds number decrease rapidly too.

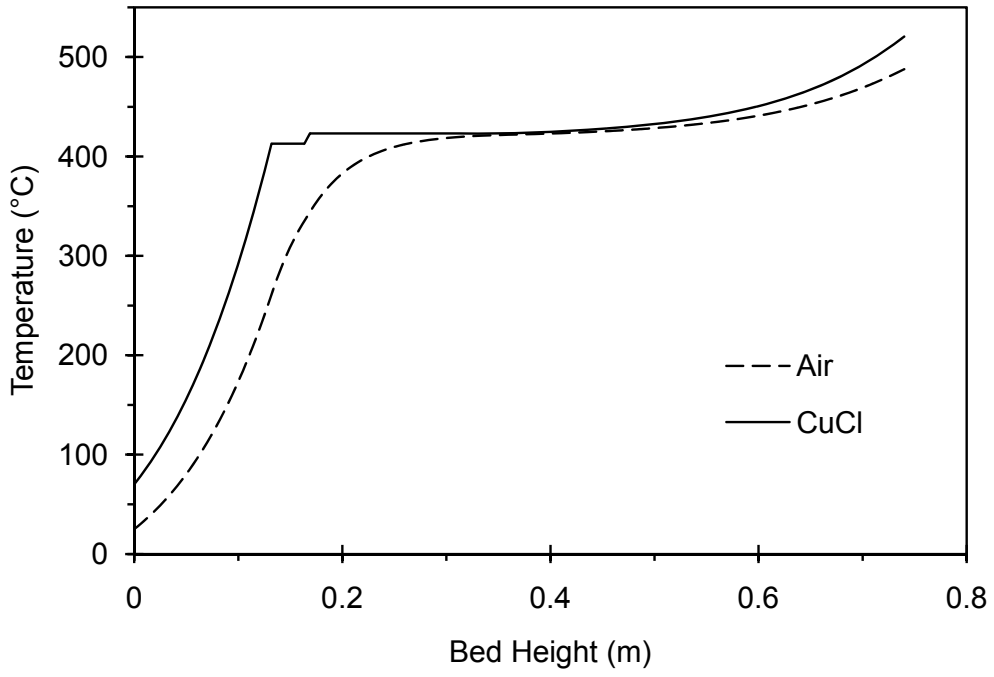


Figure 4.8 Temperature distribution for CuCl droplets with 0.5 mm diameter.

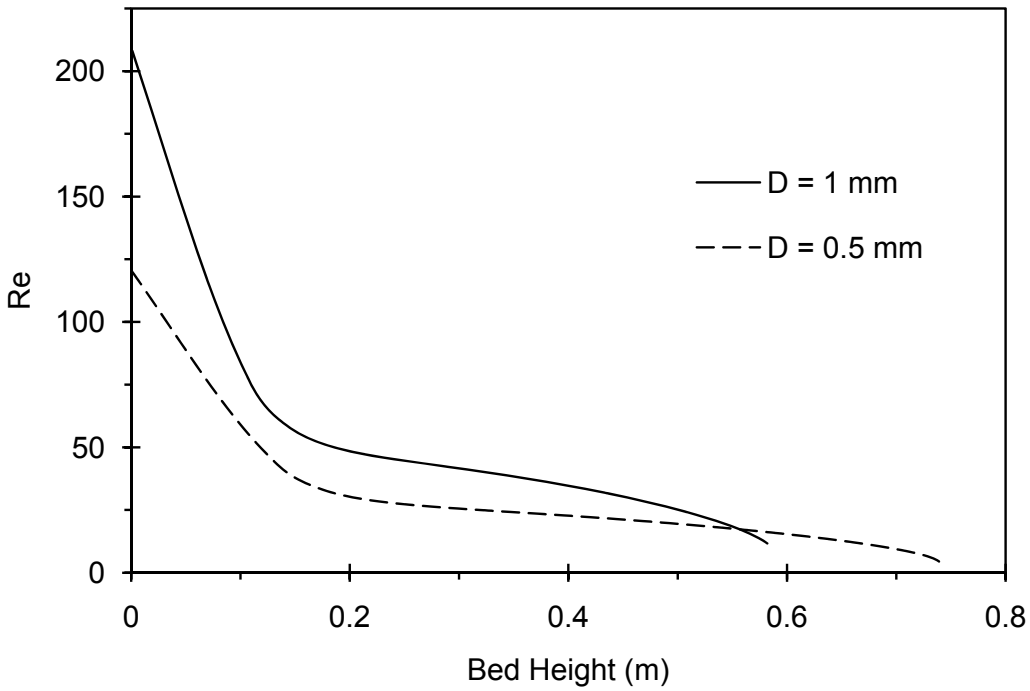


Figure 4.9 Reynolds number variation with bed height.

It is evident from the graph that even though droplets with a 0.5 mm diameter undergo much larger velocities than droplets with a 1 mm diameter. The Re numbers for the smaller droplet diameter is lower. This is because of the diameter effect, since the smaller droplet has a diameter that is half that of the large droplet. A velocity that is twice as large as that of the velocities experienced by the larger droplet diameters are required to make the smaller droplet have the same Reynolds number. But since the velocities experienced by the smaller droplet are lower than the required velocity to make Re the same, the resulting Re is lower.

Figure 4.10 shows the variation of the Nusselt number with height for droplet diameters of 1 and 0.5 mm. The variation follows closely the variation of Re number with height. This is expected since Nu is a function of Re, as shown in the correlation used to find Nu in chapter 3.

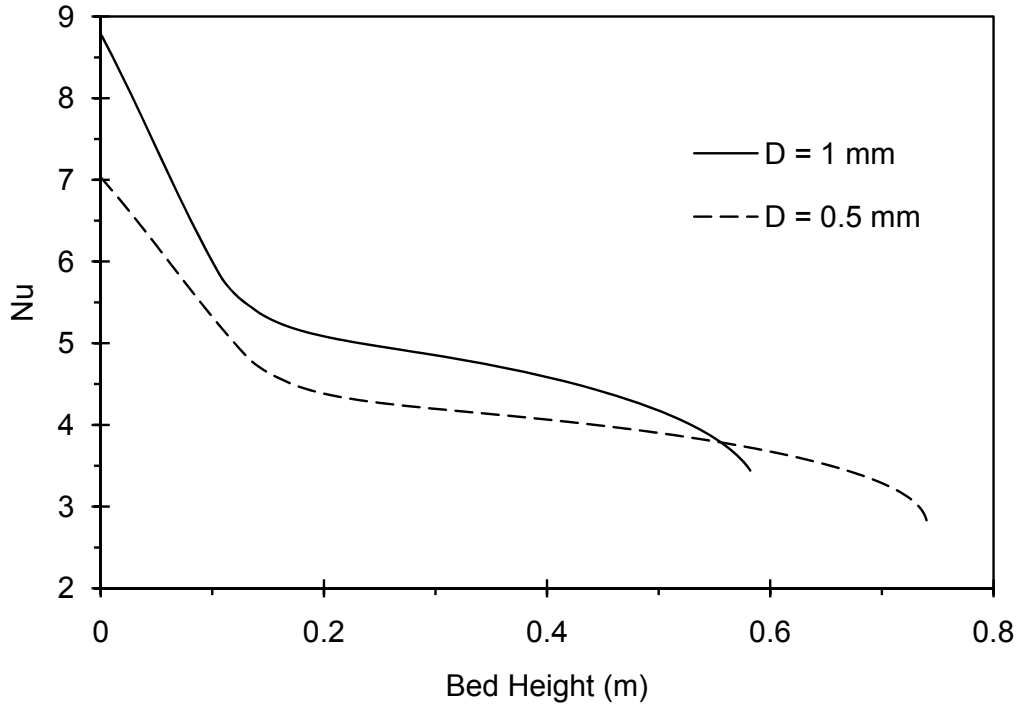


Figure 4.10 Nusselt's number variation with bed height.

Figure 4.11 shows the variation of the convection heat transfer coefficient with height for droplets with 1 and 0.5 mm diameters. From the graph, it can be noticed that droplets with a diameter of 0.5 mm have a much larger convection heat transfer coefficient than droplets with a diameter of 1 mm, even though the Nu value is very close for both droplet diameters. The reason is that the denominator used to find the convection heat transfer coefficient, equation (3.26), for a droplet with a diameter of 0.5 mm, is half that of a droplet with a diameter of 1 mm. This results in a higher convection heat transfer coefficient value.

The convection heat transfer coefficient increases initially, because of the high increase rate in the air's thermal conductivity, caused by the high increase in the air temperature. This overweighs the large decrease rate in Nu, causing the convection heat transfer coefficient to increase. The convection heat transfer coefficient starts

decreasing at an accelerated rate. This is because the air temperature increases at a slow rate in this region, making the air thermal conductivity increase at a very slow rate, while Nu decreases at a high rate. In this region, the high decrease rate in Nu overweighs the small increase rate in the thermal conductivity, making the convection heat transfer coefficient decrease with height.

Also, for the two droplet diameters, the difference between the convection heat transfer coefficients almost stays constant throughout the height. This is caused by the almost constant ratio between the droplet's diameters throughout the height.

Figure 4.12 shows the variation of the heat transfer rate for droplets with 1 and 0.5 mm diameters throughout the height of the heat exchanger. It is evident from the graph that the larger droplet diameter has a higher heat transfer rate. This is because of the area ratio between the two droplets. A droplet with a diameter of 1 mm has four times the surface area of a droplet with a 0.5 mm diameter. However, the heat transfer rate is not four times as high.

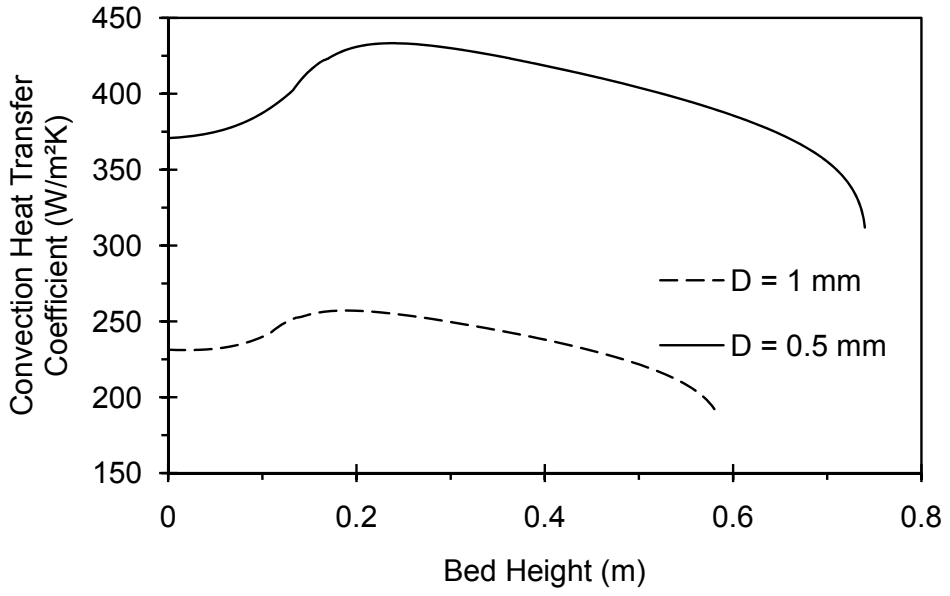


Figure 4.11 Convective heat transfer coefficient variation.

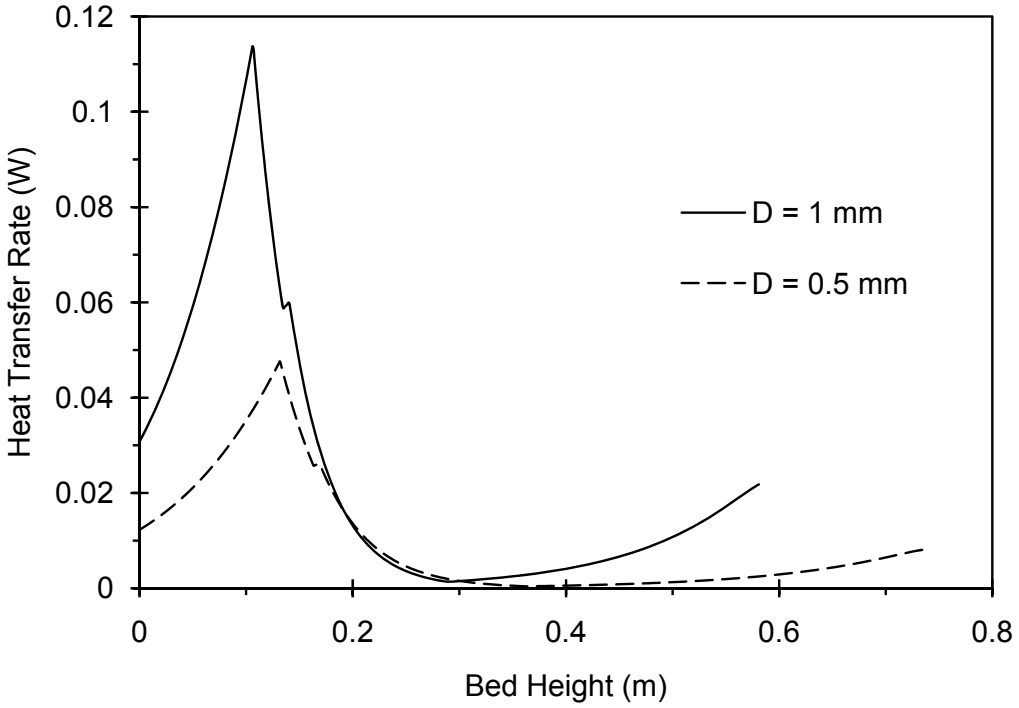


Figure 4.12 Heat transfer rate variation.

The heat transfer rate increases initially at the bottom of the heat exchanger, because of the increasing temperature difference between both streams in this region, which gives a higher potential for heat transfer. The heat transfer rate reaches a maximum value at the point where the second phase transformation ends. After this point, it starts decreasing, due to the decreasing temperature difference between both fluids in the phase transformation process. When the second sensible heat transfer process is reached, the heat transfer rate starts increasing again, due to the same reason discussed earlier. The increase in heat transfer does not last for long because the first phase transformation process is at a temperature away from the second phase transformation process by 11 degrees. In the first phase transformation process, the heat transfer rate decreases again and reaches values close to zero, because the

temperature difference reaches a value of one. Finally, the heat transfer rate increases again in the final sensible heat transfer process.

Figure 4.13 shows the heat flux variation from droplets with 1 and 0.5 mm diameters throughout the heat exchanger. The heat flux is the product of the convection heat transfer coefficient and the temperature difference. This graph shows that the heat flux from smaller droplet diameters is larger than that from large droplet diameters, as opposed to the higher heat transfer rate from larger droplet diameters, as shown previously. The larger heat flux from smaller droplet diameters occurs because of the much larger convection heat transfer coefficient than a larger diameter droplet. The heat flux follows the same trend that the heat transfer rate follows along the height of the heat exchanger. The same discussion applies as that of the heat transfer variation with height.

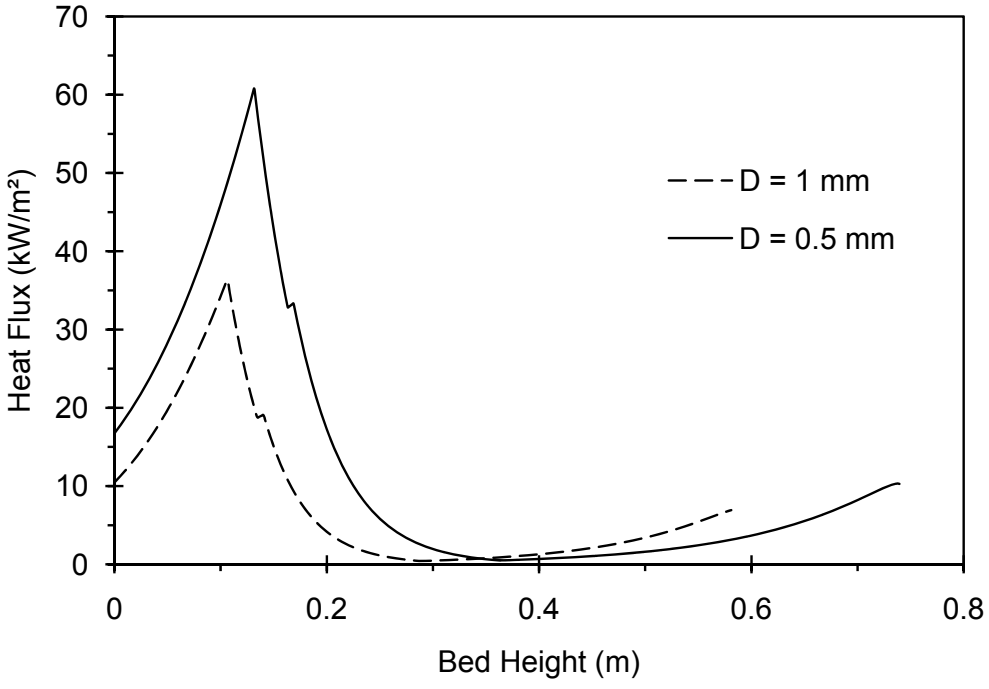


Figure 4.13 Droplet heat flux variation.

Table 4.2 shows a summary of the heat exchanger characteristics for both of the investigated cases. The number of CuCl droplets represents the number of droplets that have an equivalent mass flow rate as the case presented. The number of droplet injectors is the number of injectors at the top of the heat exchanger generating droplets. In case 1, the injector gives the droplets a velocity of 0.02 m/s, which means it has to inject 18 droplets per second. In case 2, the injector has to give the droplets a velocity of 0.07 m/s, which means it has to inject 142 droplets per second.

## 4.4 Real and Ideal Air Thermophysical Properties

A comparison is made between ideal and real air properties in this section. All properties were obtained from EES software. Figures 4.14 to 4.18 show how the properties of real air compare to that of ideal air. It can be seen that good agreement between both is obtained, so the assumption of air being an ideal gas is validated. The graphs of the density and specific volume variation with temperature, for real and ideal air, are very close to each other. For the variation of the specific heat, thermal conductivity, and dynamic viscosity with temperature, there is a slight variation between ideal and real air properties at either the lower or higher ends of the considered temperature range.

Table 4.2 Heat exchanger characteristics.

| Parameter | Case 1: Droplet Diameter of 1 mm | Case 2: Droplet Diameter of 0.5 mm |
|---|---|---|
| **CuCl Mass Flow Rate (g/s)** | 3.4 | 3.4 |
| **Air Mass Flow Rate (g/s)** | 3 | 3 |
| **CuCl Inlet Temperature (°C)** | 530 | 530 |
| **CuCl Exit Temperature (°C)** | 70 | 70 |
| **Air Inlet Temperature (°C)** | 25 | 25 |
| **Air Exit Temperature (°C)** | 493 | 493 |
| **Number of CuCl Droplets** | 1779 | 14226 |
| **CuCl Droplet Inlet Velocity (m/s)** | 0.02 | 0.07 |
| **Air Inlet Velocity (m/s)** | 0.2 | 0.2 |
| **Droplet Travel Time (s)** | 0.36 | 0.40 |
| **Number of Droplet Injectors** | 100 | 100 |
| **Heat Exchanger Height (m)** | 0.6 | 0.8 |
| **Heat Exchanger Diameter (m)** | 0.13 | 0.13 |

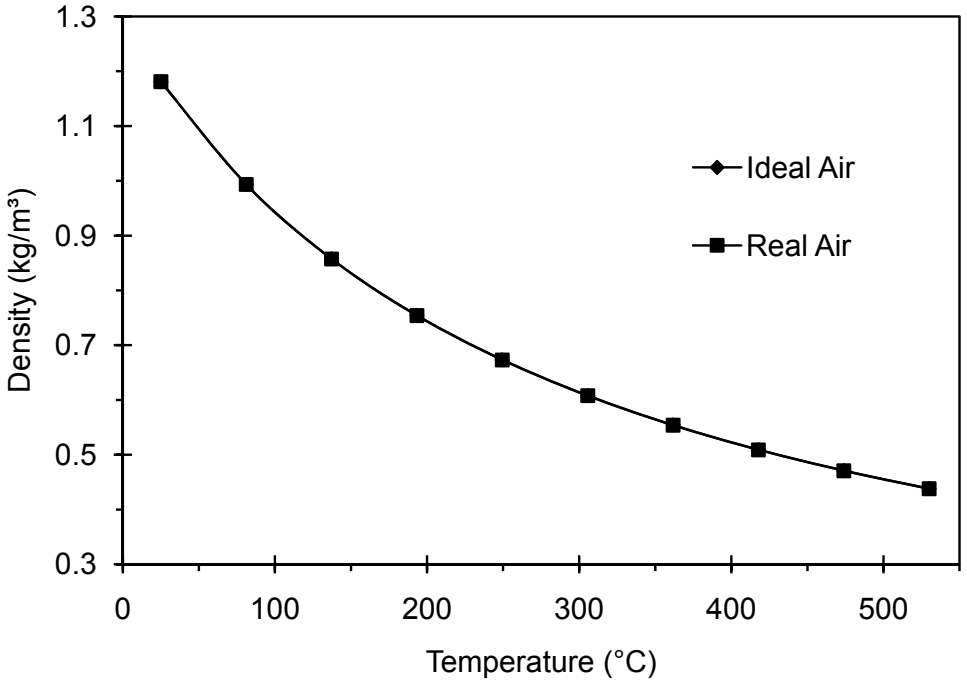


Figure 4.14 Air density variation with temperature for real and ideal air.

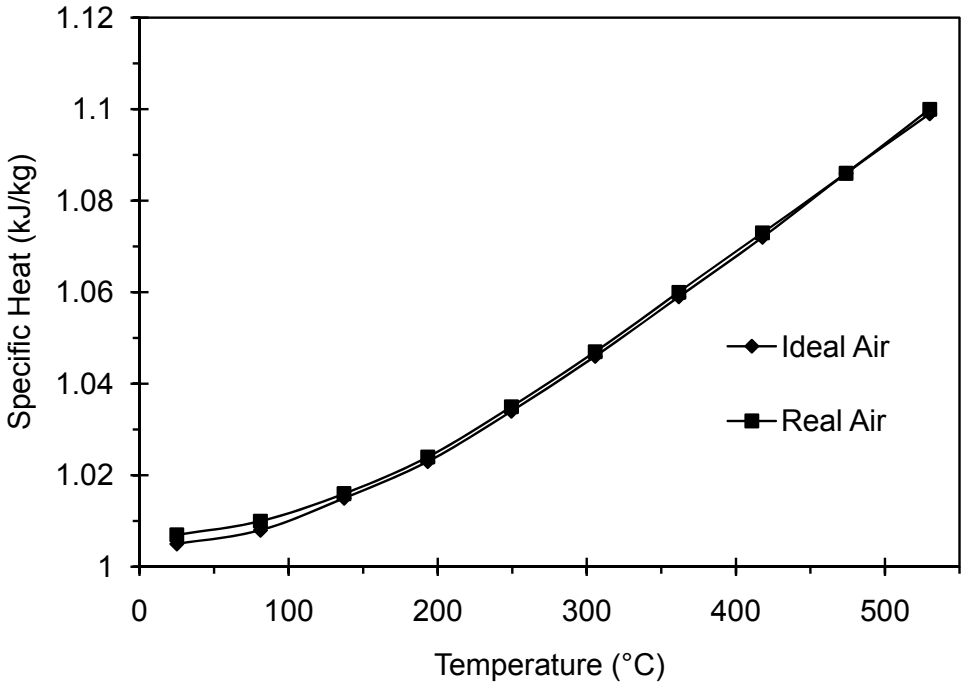


Figure 4.15 Specific heat variation with temperature for real and ideal air.

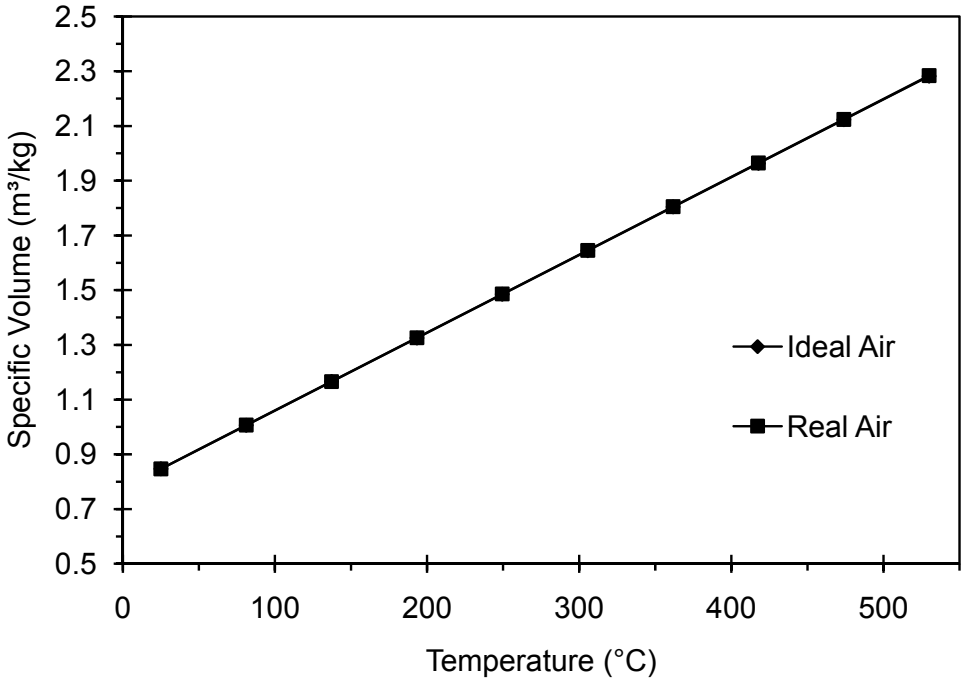


Figure 4.16 Specific volume variation with temperature for real and ideal air.

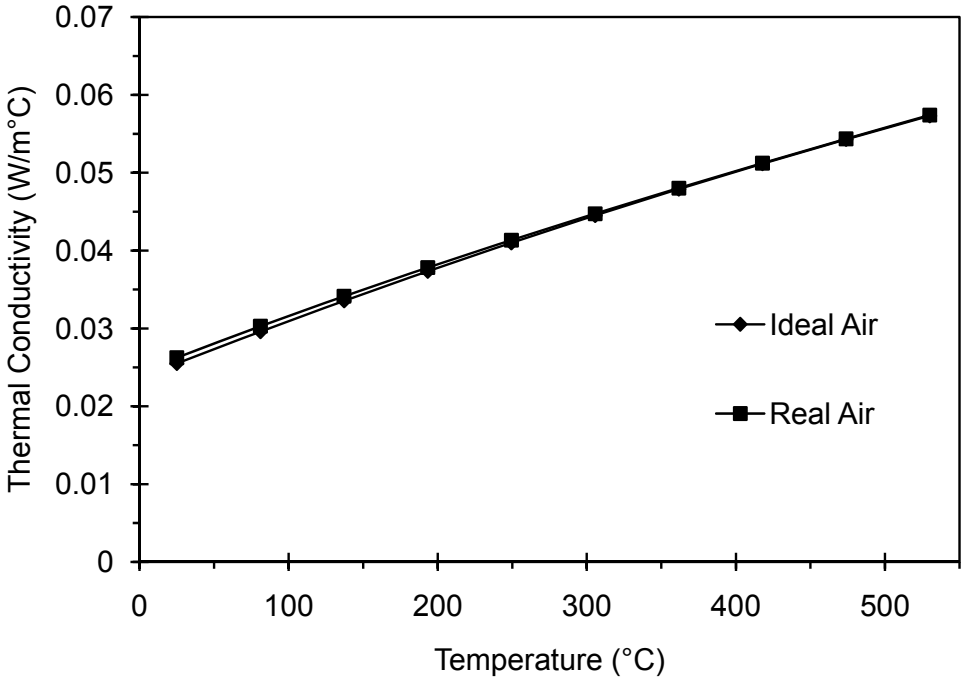


Figure 4.17 Thermal conductivity variation with temperature for real and ideal air.

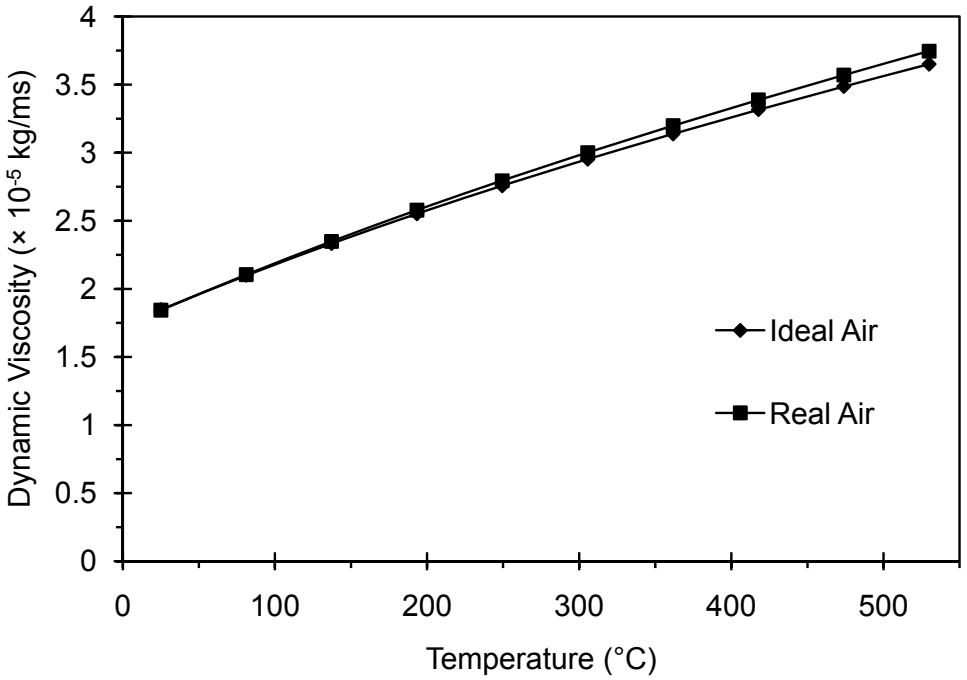


Figure 4.18 Dynamic viscosity variation with temperature for real and ideal air.

# Chapter 5

## Conclusions and Recommendations for Future Work

### 5.1 Conclusions

This thesis has examined the problem of recovering heat from molten CuCl produced from the oxygen production step in a Cu-Cl cycle for hydrogen production. The molten CuCl must be cooled before it enters the next step in the Cu-Cl cycle, which is the Cu production step in an electrochemical cell. A spray column direct contact heat exchanger is developed to recover heat and use it to provide the heat requirements of other steps. Apart from heat recovery by spraying water on a high temperature metal in continuous casting processes, this was found to be the most viable method to recover heat from a continuous stream of CuCl droplets. Other methods that might have potential for recovering heat from the molten CuCl operate in batches, such as fluidized beds.

A model for the fluid and droplet flows, as well as the heat transfer process, was developed. The simulation results of the model show that a direct contact heat exchanger can be designed with reasonable dimensions to recover thermal energy from the molten CuCl generated by a hydrogen production plant, with a capacity of 3 kg of hydrogen per day.

To achieve heat transfer in a direct contact heat exchanger, the molten CuCl is sprayed to form droplets. Two cases of droplet diameters have been investigated, 1 and 0.5 mm, and the flow and heat transfer characteristics have been compared. For

both droplet sizes, the heat exchanger was divided into five regions; three regions for sensible heat transfer, and two regions for latent heat transfer. The division of the heat exchanger into regions is due to the phase transformations of a CuCl droplet as it cools down.

For both of the analyzed cases, the inlet and exit CuCl temperatures were 530 and 70°C respectively. Air at standard ambient conditions was used to recover the energy. It had inlet and exit temperatures of 25 and 493°C. Total energy recovery by the air flow was achieved. The required height of the heat exchanger for each of the cases was 0.6 m for droplets with a diameter of 1 mm, and 0.8 m for droplets with a diameter of 0.5 mm. The major portion of the height was needed for the two heat transfer processes associated with the phase transformations of CuCl. This is very similar to the portion of area that is required by other types of heat exchangers, such as condensers and evaporators, for the latent heat process, which usually is 80 – 90% of the total area.

The proposed method of recovering the heat energy, via a direct contact heat exchanger involving countercurrent CuCl droplet and air flows, is an excellent solution to the heat recovery problem in a single step. That recovers all of the heat and maintains its quality; the exit air temperature is very close to the inlet CuCl temperature.

After comparing the overall dimensions of the heat exchanger for both of the droplet diameter cases, it was found that there is no benefit in spraying the CuCl to finer droplets. This is only for the flow case of 100 injectors, which is the case considered in the study. If more injectors are used at the top of the heat exchanger, a smaller diameter droplet may outperform the larger droplet diameter in terms of heat exchanged. This will reduce the height of the heat exchanger drastically. This is

because of the much larger heat flux from a smaller diameter droplet than a large diameter droplet.

The following are the main differences between the two examined cases:

1. Smaller droplets experience larger velocities and accelerations, due to their lower drag force, at the outlet of the heat exchanger.
2. Smaller droplets require a higher heat exchanger to recover the heat from them, under the same heat exchanger parameters.
3. The convective coefficient is much larger for smaller droplets.
4. Heat transfer rates from smaller droplets are less than from larger ones, however, the heat flux from them is much higher.

## 5.2 Recommendations for Future Research

Experimental studies of a direct contact heat exchanger, working with the conditions specified in this work, are recommended to validate the model, and find if any modifications can be made to the model, in order to improve its performance. The experimental analysis will also help in validating the assumptions used to develop the model.

A more detailed analysis of the droplet and fluid flow, and heat transfer phenomena in the heat exchanger is recommended. The detailed model should take into account real air properties instead of ideal gas properties. It should also analyze the transient heat transfer within the droplet itself, to find the temperature profile within the droplet during the phase change process, and therefore determine whether total phase change of CuCl is accomplished or not. It should also take into account the effect of the wake created by each droplet on the one that follows it, to find if this effect can be neglected or not.

Finally more research is needed to analyze and compare different methods of recovering heat from the molten CuCl, in order to find the best method for recovering heat from the molten salt. This includes future studies to determine the best configuration of injectors, number of injectors, droplet diameters, and potential dust / particle in the outlet air stream.

# References


[1] Dincer, I., Rosen, M.A., "Exergy, Energy, Environment and Sustainable Development", 1st ed., Oxford, *Elsevier*, 2007.

[2] Leon, A., "Hydrogen Technology: Mobile and Portable Applications", 1st ed., Berlin, *Springer*, 2008.

[3] Dincer, I., "Environmental and Sustainability Aspects of Hydrogen and Fuel Cell Systems", *International Journal of Energy Research*, Vol. 31, 2007, pp. 29-55.

[4] Rosen, M.A., "Thermodynamic Investigation of Hydrogen Production by Steam Methane Reforming", *International Journal of Hydrogen Energy*, Vol. 16, 1991,pp. 207-217.

[5] Gupta, R.B., "Hydrogen Fuel: Production, Transport, and Storage",ast ed., Boca Raton, *Taylor and Francis Group*, 2008.

[6] Rosen, M.A., "Thermodynamic Comparison of Hydrogen Production Processes", *International Journal of Hydrogen Energy*, Vol. 21, 1996, pp. 349-365.

[7] Rosen, M.A., Scott, D.S., "Comparative Efficiency Assessment for A Range of Hydrogen Production Processes", *International Journal of Hydrogen Energy*, Vol. 23, 1998, pp. 653-659.

[8] Wang, Z., Gabriel, K., Naterer G.F., "Thermochemical Process Heat Requirements of the Copper-Chlorine Cycle for Nuclear Based Hydrogen

Production", *29th Conference of the Canadian Nuclear Society*, Toronto, May, 2008.

[9] Simpson, A.P., Lutz, A.E., "Exergy Analysis of Hydrogen Production Via Steam Methane Reforming", *International Journal of Hydrogen Energy*, Vol. 32, 2007, pp. 4811-4820.

[10] Naterer, G.F., Gabriel, K., Wang, Z.L., Daggupati, V.N., Gravelsins, R., "Thermochemical Hydrogen Production With a Copper-Chlorine Cycle. I: Oxygen Released From Copper Oxychloride Decomposition", International Journal of Hydrogen Energy, Vol. 33, 2008, pp. 5439-5450.

[11] Richter, S., Wagner, U., "Renewable Energy", 1st ed., Berlin, *Springer*, 2008.

[12] de Jong, M., Reinders, A.H.M.E., Kok, J.B.W., Westendorp, G., "Optimizing a Steam Methane Reformer for Hydrogen Production", *International Journal of Hydrogen Production*, Vol. 34, 2009, pp. 285-292.

[13] Watanabe, H., Otaka, M., "Numerical Simulation of Coal Gasification in Entrained Flow Coal Gasifier", *Fuel*, Vol. 85, 2006, pp. 1935-1943.

[14] Yang, L., Zhang, X., Liu, S., Yu, L., Zhang, W., "Field Test of Large-Scale Hydrogen Manufacturing From Underground Coal Gasification (UCG)", *International Journal of Hydrogen Energy*, Vol. 33, 2008, pp. 1275-1285.

[15] Dutta, S., "Technology Assessment of Advanced Electrolytic Hydrogen Production", *International Journal of Hydrogen Energy*, Vol. 15, 1990, pp. 379−386.

[16] Brisse, A., Schefold, J., Zahid, M., "High Temperature Water Electrolysis in Solid Oxide Cells", *International Journal of Hydrogen Energy*, Vol. 33, 2008, pp. 5375-5382.

[17] Shimizu, N., Hotta, S., Sekiya, T., Oda, O., "A Novel Method of Hydrogen Generation by Water Electrolysis Using an Ultra-Short-Pulse Power Supply", *Journal of Applied Electrochemistry*, Vol. 36, 2006, pp. 419-423.

[18] Stojic, D.L., Milica P.M., Sofija P.S., Miljanic, S.S., "Hydrogen Generation from Water Electrolysis — Possibilities of Energy SavinG", *Journal of Power Sources*, Vol. 118, 2003, pp. 315-319.

[19] Fishtik, I., Datta, R., "Systematic Generation of Thermochemical Cycles for Water Splitting", *Computers and Chemical Engineering*, Vol. 32, 2008, pp. 1625-1634.

[20] Keefe, D.O., Allen, C., Besenbruch, G., Brown, L., Norman, J., Sharp, R., "Preliminary Results from Bench-Scale Testing of a Sulfur-Iodine Thermochemical Water Splitting Cycle", *International Journal of Hydrogen Energy*, Vol. 7, 1982, pp. 381−392.

[21] Onuki, K., Inagaki, Y., Hino, R., Tachibana, Y., "Research and Development on Nuclear Hydrogen Production Using HTGR at JAERI", *Progress in Nuclear Energy*, Vol. 47, 2005, pp. 496−503.

[22] Grimes, C.A., Varghese, K.O., Ranjan, S., "Light, Water, Hydrogen: The Solar Generation of Hydrogen by Water Photoelectrolysis.", 1st ed., New York, *Springer*, 2008

[23] Yildiz, B., Kazimi, M. S., "Efficiency of Hydrogen Production Systems Using Alternative Nuclear Energy Technologies", *International Journal of Hydrogen Energy*, Vol. 31, 2006, pp. 77-92.

[24] Xinxin, W., Kaoru, O., "Thermochemical Water Splitting for Hydrogen Production Utilizing Nuclear Heat from an HTGR", *Tsinghua Science And Technology*, Vol. 10, 2005, pp. 270-276.

[25] Naterer, G.F., Daggupati, V.N., Marin, G., Gabriel, K.S., Wang, Z.L., "Thermochemical Hydrogen Productin with a Copper-Chlorine Cycle, II: Flashing and Drying of Aqueous Cupric Chloride", *International Journal of Hydrogen Energy*, Vol. 33, 2008, pp. 5451-5459.

[26] Rosen, M.A., Naterer, G.F., Sadhankar, R., Suppiah, S., "Nuclear-Based Hydrogen Production With Thermochemical Copper-Chlorine Cycle and supercritical Water Reactor", *Canadian Hydrogen Association Workshop*, Montreal, October, 2006.

[27] Wanga, Z., Naterer, G.F., Gabriel, K., "Multiphase Reactor Scale-up for Cu–Cl Thermochemical Hydrogen Production", *International Journal of Hydrogen Energy*, Vol. 33, 2008, pp. 6934-6946.

[28] Orhan, M.F., Dincer, I., Naterer, G.F., "Cost Analysis of a Thermochemical Cu–Cl Pilot Plant for Nuclear-Based Hydrogen Production", *International Journal of Hydrogen Energy*, Vol. 33, 2008, pp. 6006-6020.

[29] Botterud, A., Yildiz, B., Conzelmann, G., Petri, M. C., "Nuclear Hydrogen: An Assesment of Product Flexibility and Market Viability", *Energy Policy*, Vol. 36, 2008, pp. 3961-3973.

[30] Kimura, H., Tekeuchi, Y., Yamamoto, Y., Konishi, S., "Hydrogen Production from Biomass using Nuclear Fusion Energy", *21st IEEE/NPS Symposium on Fusion Engineering*, Knoxville, September, 2005.

[31] Torjman, M., Shaaban, H., "Nuclear Energy as a Primary Source for a Clean Hydrogen Energy System", *Energy Conversion and Managment*, Vol. 39, 1998, pp. 27-32.

[32] Verfondern, K., Von Lens, W., "Past and Present Research in Europe on the Production of Nuclear Hydrogen with HTGR", *Progress in Nuclear Energy*, Vol. 47, 2005, pp. 1-4.

[33] Hori, M., Matsui, K., Tashimo, M., Yasuda, I., "Synergistic Hydrogen Production by Nuclear-Heated Steam Reforming of Fossil Fuels", *Progress in Nuclear Energy*, Vol. 47, 2005, pp. 519-526.

[34] Schlapbach, L., Zuttle, A., "Hydrogen-Storage Materials for Mobile Applications", *Nature*, Vol. 414, 2001, pp. 353-358.

[35] Cumalioglu, I., Ertas, E., Ma, Y., Maxwell, T., "Hydrogen Storage", *Journal of Fuel Cell Science and Technology*, Vol. 5, 2008, pp. 1-10.

[36] Kandavel, M., Bhat, V.V., Rougier, A., Aymard, L., Nazri, G.A., Tarascon, J.M., "Improvement of Hydrogen Storage Properties of the AB2 Laves Phase Alloys for Automotive Application", *International Journal of Hydrogen Energy*, Vol. 33, 2008, pp. 3754-3761.

[37] Damle, A., Ordaz, G., Alkire, J., "Development of Regenerable High Capacity Boron Nitrogen Hydrides as Hydrogen Storage Materials", *U.S. Department of Energy Report*, Washington, 2007, pp. 460-463.

[38] Onuki, A., Kanatani, K., "Droplet Motion with Phase Change in a Temperature Gradient", *Physical Review E*, Vol. 72, 2005, pp. 1-11.

[39] de Villeneuve, V., Aarts, D., Lekkerkerker, H., "Comparing the Approach of a Rigid Sphere and a Deformable Droplet Towards a Deformable Fluid Surface", *Colloids and Surfaces*, Vols. 282, 2006, pp. 61-67.

[40] Masoudi, M., Sirignano, W.A., "The Influence of an Advecting Vortex on the Heat Transfer to a Liquid Droplet", *International Journal of Heat and Mass Transfer*, Vol. 40, 1997, pp. 3663-3673.

[41] Quan, S., Schmidt, D., "Direct Numerical Study of a Liquid Droplet Impulsively Accelerated by Gaseous Flow", *Physics of Fluids*, Vol. 18, 2006, pp. 1-9.

[42] Ni, M., Komori, S., Morley, N., "Direct Simulation of Falling Droplet in a Closed Channel", *International Journal of Heat and Mass Transfer*, Vol. 49, 2006, pp. 366-376.

[43] Feng, Z., Michaelides, E.E., "A Numerical Study on the Transient Heat Transfer from a Sphere at High Reynolds and Peclet Numbers", *International Journal of Heat and Mass Transfer*, Vol. 43, 2000, pp. 219-229.

[44] Feng, Z., Michaelides, E.E., "Heat and Mass Transfer Coefficients of Viscous Spheres", *International Journal of Heat and Mass Transfer*, Vol. 44, 2001, pp. 4445-4454.

[45] Kartushinskii, A., Michaelides, E., Rudi, Y., "Numerical Modeling of Gas-Particle Flows in Vertical Pipes and the Particle Collision Effect", *Fluid Dynamics*, Vol. 39, 2004, pp. 748-755.

[46] Feng, Z., Michaelides, E.E., Scibilia, M., "The Energy Equation of a Sphere in an Unsteady and Nonuniform Temperature Field", *Revue Generale de Thermique*, Vol. 35, 1996, pp. 5-13.

[47] Kadja, M., Bergeles, G., "Modelling of Slurry Droplet Drying", *Applied Thermal Engineering*, Vol. 23, 2003, pp. 829-844.

[48] Whitaker, S., "Forced Convection Heat Transfer Correlations for Flow in Pipes, Past Flat Plates, Single Cylinders, Single Spheres, and for Flow in Packed Beds and Tube Bundles", *AIChE Journal*, Vol. 18, 1972, pp. 361-371.

[49] Levi, C.G., Mehrabian, R., "Heat Flow During Rapid Solidification of Undercooled Metal Droplets", *Metallurgical Transactions A*, Vol. 13, 1982, pp. 221-234.

[50] Mitrovic, J., Stephan, K., "Mean Fluid Temperatures in Direct Contact Heat Exchangers without Phase Change", *International Journal of Heat and Mass Transfer*, Vol. 39, 1996, pp. 2745-2750.

[51] Shimuzu, A., Yokomine, T., Nagafuchi, T., "Development of Gas-Solid Direct Contact Heat Exchanger by Use of Axial Flow Cyclone", *International Journal of Heat and Mass Transfer*, Vol. 47, 2004, pp. 4601-4614.

[52] Daggupati, V.N., Naterer, G.F., Gabriel, K.S., "Heat Recovery with Low Temperature Spray Drying for Thermochemical Hydrogen Production", *Advanced Computational Methods in Heat Transfer X*, Vol. 61, 2008, pp. 105-114.

[53] Errera, M., Milanez, F., "Thermodynamic Analysis of a Coke Dry Quenching Unit", *Energy Conversion and Management*, Vol. 41, 2000, pp. 109-127.

[54] Zarrinehkafsh, M.T., Sadrameli, S.M., "Simulation of Fixed Bed Regenerative Heat Exchangers for Flue Gas Heat Recovery", *Applied Thermal Engineering*, Vol. 24, 2004, pp. 373-382.

[55] Caputo, A.C., Pelagagge, P.M., "Heat Recovery from Moving Cooling Beds: Transient Modeling by Dynamic Simulation", *Proceedings of the Thirty-Second Intersociety Energy Conversion Engineering Conference*, Honululu, July, 1997, Vol. 3, pp. 1550-1555.

[56] Gandjalikhan Nassab, S.A., "Transient Heat Transfer Characteristics of an Energy Recovery System using a Porous Medium", *Journal of Power and Energy*, Vol. 216, 2002, pp. 387-394.

[57] Bisio, G., Cartesegna, M., Rubatto, G., "Energy Recovery by Evaporative Cooling in Several Plants of the Iron and Steel Industry", *Proceedings of the 37th Intersociety Energy Conversion Engineering Conference*, Washington, July, 2004, pp. 751-756.

[58] Skiepko, T., Shah, R., "Modeling and Effect of Leakages on Heat Transfer Performance of Fixed Matrix Regenerators", *International Journal of Heat and Mass Transfer*, Vol. 48, 2005, pp. 1608-1632.

[59] Pasini, S., Ghezzi, I., Andriani, R., Ferri, L.D.A., "Heat Recovery from Aircraft Engines", *Processdings of the 35th Intersociety Energy Conversion Engineering Conference and Exhibit*, Las Vegas, July, 2000, Vol. 1, pp. 546-553.

[60] Michaelides, E.E., "Particles, Bubbles and Drops: Their Motion, Heat and Mass Transfer", 1st ed., Singapore, *World Scientific Publishing*, 2006.

[61] Bejan, A., Kraus, A.D., "Heat Transfer Handbook", 1st ed., Hoboken, *John Wiley and Sons, Inc.*, 2003.

[62] Mathias, P.M., "Aspen Plus Model for Solubilities in the $CuCl_2$-CuCl-HCl-$H_2O$ System", *Argonne National Laboratory Report*, Argonne, May, 2007.

[63] Department of Chemistry, Moscow State University, "*Thermodynamic Propertiesof Compounds*", http://www.chem.msu.su/rus/weldept.html#lib, August, 2009.

[64] Slact, G.A., Andersson, P., "Pressure and Temperature Effects on the Thermal Conductivity of CuCl", *Physical Review B*, Vol. 26, 1982, pp. 1873-1884.

[65] Incropera, F.P., Dewitt, D.P., Bergman, T.L., Lavine, A.S., "Fundamentals of Heat and Mass Transfer', 6th ed., Hoboken, *John Wiley and Sons, Inc.*, 2007.